

Increase with energy of parton transverse momenta in the fragmentation region in DIS and related phenomena.

B. Blok

Department of Physics, Technion—Israel Institute of Technology, 32000 Haifa, Israel

L. Frankfurt

*School of Physics and Astronomy, Raymond and Beverly Sackler Faculty of Exact Sciences,
Tel Aviv University, 69978 Tel Aviv, Israel*

M. Strikman

Physics Department, Penn State University, University Park, PA, USA

Abstract

The dipole and the DGLAP approximations are combined with the k_t factorization theorem to demonstrate the fundamental property of pQCD: smaller is the size of the colorless quark-gluon configurations in the fragmentation region, more rapid is the increase of its interaction with the target as a function of energy. First, we consider two closely related properties of the wave function of the projectile (i) the transverse momenta of the quark(antiquark) within the $q\bar{q}$ pair, produced in the fragmentation region by the strongly virtual photon, increase with the decrease of x for fixed Q^2 , (ii) increase of the relative contribution of pQCD to the structure functions as compared to soft QCD contribution at central impact parameters due to a rapid increase with energy of the cross section of interaction of small dipoles. Practical consequences of these effects are presented for the cases of the cross sections of DIS and DVCS. We predict that the ratio of DVCS to DIS amplitudes should very slowly approach one from above at very large collision energies. Second, we study a closely related phenomenon of the increase of the transverse momenta with the energy of the characteristic transverse momenta of the gluon/quark configurations responsible for the transition to the black disk regime. We discuss the impact of this phenomena on the slowing of the dependence on the initial energy of the coherence length. We demonstrate that a rapid projectile has the biconcave shape, which is different from the expectations of the preQCD parton model where a fast hadron has a pancake shape. We show that the increase of the transverse momenta leads to a new expression for the total cross section of a DIS scattering at very large energies, relevant to LHeC and LHC. We discuss the impact of the discovered phenomena on the hard processes in pp collisions, and on the dominance of different phases of chiral and conformal symmetries in the central and peripheral pp, pA, and AA collisions.

I. INTRODUCTION.

The leading order dipole approximation for the high energy processes in QCD developed in Ref. [1], cf. also Refs. [2, 3, 4, 5, 6], is the generalization of the pQCD improved parton model to the target rest frame description. The leading order dipole approximation provides the solution of the equations of QCD in the kinematics of fixed and small, but not too small $x = Q^2/\nu$ and not very small Q^2 .

The main aim of the current paper is the study of the properties of the DIS processes in the fragmentation region. In particular, we study two closely related properties of the wave function of the projectile.

First, we consider two properties of the perturbative QCD (pQCD) wave function of the projectile: (i) we find the increase with energy ($1/x$) of the transverse momenta (k_t) of the quark(antiquark) within the $q\bar{q}$ pair produced in the fragmentation region by the strongly virtual photon, (ii) we see the increase of the relative contribution of pQCD to the structure functions as compared to the soft QCD contribution at central impact parameters due to a rapid increase with energy of the cross section of interaction of small dipoles. We show that at sufficiently high energies the transverse momenta k_t become larger than $Q^2/4$. As a result a new pQCD regime different from the conventional DGLAP [7], appears at these energies. The reason is that the ordering in transverse momenta that led to large $\log(Q^2/\Lambda^2)$ is not valid any more. Practical consequences of these effects are presented for the cases of the cross sections of DIS and DVCS. We predict that the ratio of DVCS to DIS amplitudes should decrease with energy and very slowly approach one from above at very large collision energies. In addition the ratio $\sigma_L/\sigma_t \propto Q^2/(4k_t^2)$ will also slowly decrease with energy. Technically these effects follow from the more rapid increase with the energy of the pQCD interaction for smaller dipole and the k_t factorization theorem [8, 9].

Second, we study a closely related phenomenon of the increase with the energy of the characteristic transverse momenta of the gluon/quark configurations in the wave function of the projectile responsible for the transition to the black disk/Froissart (BDR) regime. We discuss the impact of this phenomena on the slowing of the rate of increase of the coherence length as a function of energy. The most striking implication of our analysis is the change of the space structure of the wave packet describing a rapid hadron. In the classical multiperipheral picture of Gribov a hadron has a shape of a pancake of the longitudinal size $1/\mu$ (where μ is the scale of soft QCD) which does not depend on the incident energy [10]. On the contrary, we find the biconcave shape for the rapid hadron in pQCD with the minimal longitudinal length (that corresponds to small impact parameter b) decreasing with increase of energy and being smaller for the nuclei than for the nucleons.

The known rate of increase of the black disk regime momenta leads to the generalization of the old Gribov formula for the total DIS cross section in the black disk regime. We are able to establish an overall coefficient in the cross section dependence on the $\log^3(1/x)$ in the black disk regime. We determine the relative contributions of pQCD and black disk regime into the total small dipole DIS cross section at high energies. This new expression for the total cross section of a DIS scattering at very large energies is relevant to LHeC and LHC.

It is worth noting that the effect of the increase of the transverse momenta in the fragmentation region in pQCD found in this paper is very different from the seemingly similar

effect found in the leading $\alpha_s \log(x_0/x)$ BFKL approximation[11]: for the central rapidity kinematics $\log^2(k_t^2/k_{t0}^2) \propto \log(s/s_0)$. The latter is the property of the radiation within a ladder, i.e. of a diffusion in the space of the transverse momenta [11]. Indeed, it has been known for some time already that if we look at characteristic transverse momenta in a rung with a fixed number N in BFKL ladder, than in the multiregge kinematics the transverse momenta do not depend on energy. This fact follows from the derivation of Lipatov diffusion equation, where $\log(k_t^2/k_{t0}^2) \propto N$ -the number of the rung under study. The Lipatov diffusion arises since a number of rungs N in the ladder increases with the rapidity Y . An alternative proof that the transverse momenta do not rise in multiregge kinematics with a fixed number of rungs has been given in Ref. [12]. On the other hand the property we are dealing here with is the value of the transverse momenta in the wave function of the projectile.

The rapid increase with the energy of the characteristic transverse scales in the fragmentation region in the black disk regime has been found first in Refs. [13, 14, 15, 16]. The prediction of the increase with energy of the transverse momenta in the impact factor, in the kinematical domain where methods of the pQCD are still applicable can be considered as a precursor of the black disk regime indicating the possibility of the smooth matching between the pQCD and black disk regimes.

The characteristic feature of the LO dipole solution is the approximate Bjorken scaling for the structure functions of DIS, i.e. the two dimensional conformal invariance for the moments of the structure functions. In this approximation as well as within the leading $\log(x_0/x)$ approximation, the transverse momenta of quarks within the dipole produced by the local electroweak current are restricted by the virtuality of the external field:

$$\Lambda^2 \leq k_t^2 \leq Q^2/4. \quad (1.1)$$

Here $\Lambda \equiv \Lambda_{QCD} = 300$ Mev is a QCD scale. It follows from the QCD factorization theorem proved in Refs. [8, 9] that within this kinematical range the smaller transverse size d of the configuration (the transverse distance between the constituents of the dipole) corresponds to a more rapid increase of its interaction with the collision energy:

$$\sigma = \alpha_s(c/d^2)F^2 \frac{\pi^2}{4} d^2 x G(x, c/d^2), \quad (1.2)$$

here $F^2 = 4/3$ or $9/4$ depends whether the dipole consists of color triplet or color octet constituents and is a $SU(3)$ Casimir operator, G is an integrated gluon distribution function and c is a parameter $c = 4 \div 9$. It is well known in the DGLAP approximation that the structure function $G(x, Q^2)$ increases more rapidly with $1/x$ at larger Q^2 . This property agrees well with the recent HERA data.

Our main result is that the median transverse momenta k_t^2 and invariant masses of the leading $q\bar{q}$ pair in the fragmentation region in the pQCD regime grow as

$$\begin{aligned} k_t^2 &\sim a(Q^2)/(x_0/x)^{\lambda(Q^2)}, \\ M^2 &\sim b(Q^2)/(x_0/x)^{\lambda_M(Q^2)}. \end{aligned} \quad (1.3)$$

Here k_t^2 and M^2 are the median squared transverse momentum and invariant mass of the quark-antiquark pair in the fragmentation region. (The median means that the configurations with the momentum/masses less than the median one contribute half of the total

crosssection). The exponential factors λ and λ_M are both approximately ~ 0.1 . These factors are weakly dependent on the external virtuality Q^2 . Their exact values also depend on the details of the process, i.e. whether we consider the DIS process with longitudinal or transverse photons, as well as on the model and approximation used. This dependence, however, turns out to be very mild. The exact form of $\lambda(Q^2)$, and $\lambda_M(Q^2)$ is given below.

The function $b(Q^2) \sim a(Q^2)/4$ for longitudinal photons due to relation

$$M^2 = \frac{k_t^2 + m_q^2}{z(1-z)}, \quad (1.4)$$

and the dominance of the $z = 1/2$ configurations. For transverse photons however $a(Q^2) \ll b(Q^2)$ for realistic energies due a dominant contributions of configurations with $z \sim 0, 1$ in the total crosssections, i.e. $M^2 \gg 4k_t^2$ due to the relation 1.4 (z is the fraction of the total momentum of the dipole carried by one of its constituents). The characteristic invariant masses of transverse $q\bar{q}$ pair are of the order Q^2 at realistic energies.

We carry out the calculations in a wide region of a phase space:

$$10^{-7} < x < 10^{-2}, \quad 3 \text{ GeV}^2 < Q^2 < 100 \text{ GeV}^2. \quad (1.5)$$

We also obtain the increase of the median transverse momenta and invariant masses for the jet distributions for both longitudinal and transverse photons.

Although the increase of the transverse momenta in the fragmentation region was obtained in this paper in the LO approximation of pQCD it should be valid in the NLO as well. Indeed, it is known that the NLO radiative corrections to the impact factor are small [17, 18]. There are indeed large radiative corrections to the ladder however these corrections are already included in the LO CTEQ functions, that were matched to phenomenological data for the experimentally studied region of Q^2, x .

Let us note that the transverse momenta for the case of the transverse photons were calculated in the framework of the perturbative QCD. In order to ensure separation from soft physics (the AJM model), we calculated the average parton momenta with the cutoff $k_t^2 \sim 0.35 \text{ GeV}^2$. The relative contribution of the AJ quickly decreases with energy, although it is still considerable at HERA energies and Q^2 few GeV^2 .

Finally, we discuss the possible applications of our results to pp, pA collisions at the LHC. We explain that characteristic phenomena at central impact parameters are the blackening of the interactions, the increase with the energy of the parton momenta, and suppression of soft QCD contributions. At sufficiently large energies the collisions at central impact parameters will be dominated by a phase with unbroken chiral and conformal symmetries. On the contrary, the peripheral collisions will be dominated by a phase with the spontaneously broken symmetries. Applicability of this picture to QCD physics at LHC will be subject of further research.

The paper is organized in the following way. First, in section 2 we derive the spectral representation for the total crosssection of the DIS. The derivation is done within the framework of dipole model and k_t factorization and generalizes LO DGLAP [7] and BFKL [11] approximations. Next in section 3 we derive eq. 1.3 in double log approximation. This derivation has an advantage that the increase of the transverse momenta can be seen analytically, in a model independent way. Next, in section 4 we derive eq. 1.3 in LO approximation using CTEQ5 and CTEQ6 structure functions. We find the kinematical boundary of the new pQCD regime. We also discuss the influence of the soft (AJ) contributions on our results.

In section 5 we applied our results to DCVS processes and study the dependence of the cross-section of these processes on Q^2 and energy x_B . In section 6 we derive the generalisation of Gribov formulae— the formula for total DIS cross-section in the black disk region, that takes into account the rapid rise of the transverse momenta in the fragmentation region in the black disk regime. In section 7 we study the coherence length and the space-time form of the nucleons/nuclei in the black disk regime. In section 8 we discuss the experimental consequences of our results.

Some properties of the dipole approximation in QCD and DIS we use are discussed in appendixes. In appendix A we remind the reader the basic ideas of the derivation of the dipole model, in particular we give a detailed derivation of the momentum representation of the total crosssection. In appendix B we remind the reader the basic formulae of the AJM model. In appendix C we recalculate the characteristic transverse momenta for the black disk regime, using CTEQ6 distribution functions and two-gluon nucleon formfactor parametrization from ref. [13, 16]. In appendix D we present the parametrizations of the structure functions that we use in this paper. In appendix E we present some interpolation formulae that describe the data on median momenta as function of x and Q^2 as described in tables 1,2.

II. THE TARGET REST FRAME DESCRIPTION.

In this section we shall use the dipole approximation to derive the momentum representation for the total cross-sections of the DIS for both transverse and longitudinal photons. Within the LO approximation the QCD factorization theorem allows to express the total cross section of the scattering of the longitudinally polarized photon with virtuality $Q^2 \gg \Lambda_{QCD}^2$ off a hadron target as the convolution of the square of the virtual photon wave function calculated in the dipole approximation and the cross section of the dipole scattering off a hadron [1, 5, 19, 20]. In the target rest frame the cross section for the scattering of longitudinally polarized photon has the form (see appendix A in this paper for the detailed derivation of this formula):

$$\sigma(\gamma_L^* + T \rightarrow X) = \frac{e^2}{12\pi^2} \int d^2k_t dz \langle \psi_{\gamma_L^*}(k_t, z) | \sigma(s, k_t^2) | \psi_{\gamma_L^*}(k_t, z) \rangle. \quad (2.1)$$

Here σ is the dipole cross section operator:

$$\sigma = F^2 \cdot \pi^2 \alpha_s (4k_t^2) (-\vec{\Delta}_t) \cdot \tilde{x} G(\tilde{x} = (M^2 + Q^2)/s, 4k_t^2), \quad (2.2)$$

$\vec{\Delta}_t$ is the two dimensional Laplace operator in the space of the transverse momenta, and M^2 is the invariant mass squared of the dipole. In the coordinate representation σ is just a number function, and not a differential operator as in the momentum representation.

In the leading $\log(x_0/x)$ approximation a similar equation arises where the cross section is expressed in terms of convolution of impact factor and unintegrated gluon density. In practice, both equations should give close results. Integrating by parts over k_t it is easy to rewrite Eq. 2.1 with the LO accuracy in the form where the integrand is explicitly positive:

$$\sigma(\gamma_L^* + T \rightarrow X) = \frac{e^2}{12\pi^2} \int \alpha_s(4k_t^2) d^2k_t dz \langle \nabla \psi_{\gamma_L^*}(k_t, z) | f(s, z, k_t^2) | \nabla \psi_{\gamma_L^*}(k_t, z) \rangle, \quad (2.3)$$

here

$$f = (4\pi^2/3) \alpha_s(4k_t^2) \tilde{x} G(\tilde{x}, 4k_t^2). \quad (2.4)$$

In the derivation we use the boundary conditions that follow from the fact that the photon wave function decreases rapidly in the $k_t^2 \rightarrow \infty$ limit and that the contribution of small k_t is the higher twist effect (see Appendix A for details).

The cross section of the interaction of the longitudinal photon can be rewritten in the form of spectral representation by explicitly differentiating the photon wave function :

$$\sigma_L(x, Q^2) = 6\pi \frac{\pi\alpha_{\text{e.m.}} \sum e_q^2 F^2 Q^2}{12} \int dM^2 \int dz \alpha_s(4M^2 z(1-z)) \frac{M^2}{(M^2 + Q^2)^4} \cdot g(\tilde{x}, M^2). \quad (2.5)$$

Eqs.2.3, 2.5 follow from the k_t factorization theorem for high energy processes. Here $g(x, Q^2) = xG(x, Q^2)$. Thus Eq.2.5 is the generalization of the DGLAP approximation to the domain of high energies where the processes with large and increasing with energy M^2 play an important role.

Note that in Eq. 2.5 the dependence on z comes explicitly only in the argument of the coupling constant. Practically, for the dominant configurations $z \sim 1/2$ (and hence $4k_t^2 \approx M^2$). Then the dependence on z in Eq. 2.5 is absent and one can consider Eq. 2.5 (with $z=1/2$) as a spectral representation of a electroproduction amplitude for longitudinal photons. The spectral representation of the electroproduction amplitude over M^2 is a general property of a quantum field theory at large energies, where the coherence length significantly exceeds the radius of the target T [21, 22]. The DGLAP approximation ensures additional general property: the smaller size of the configuration in the wave function of the projectile photon leads to the smaller interaction with the target, but this interaction increases with the energy more rapidly. Such spectral representation is not valid for transverse photons due to the AJM effects, since the configurations with smaller z dominate (see below), and the integrand in the corresponding equation contains the contribution of different configurations (contrary to the preQCD spectral expansions).

Eq. 2.1 can be equivalently rewritten in terms of integration in k_t^2 and z as

$$\sigma_L(x, Q^2) = 6\pi \frac{\pi\alpha_{\text{e.m.}} \sum e_q^2 F^2 Q^2}{12} \int dk_t^2 \alpha_s(4k_t^2) z^2 (1-z)^2 \frac{k_t^2}{(k_t^2 + Q^2 z(1-z))^4} \cdot g(\tilde{x}, 4k_t^2). \quad (2.6)$$

where \tilde{x} is given by $(k_t^2 / ((z(1-z)) + Q^2)) / s$. Here we take into account explicitly the (rather weak) z -dependence of the integrand.

In the NLO approximation the structure of formulae should be the same except the appearance of the additional $q\bar{q}g, \dots$ components in the wave function of photon due to the necessity to take into account the QCD evolution of the photon wave function [19].

The similar derivation can be made for the scattering of transverse photon in configurations of spatially small size. In this case the contribution of small k_t region (Aligned Jet Model contribution) is comparable to the pQCD one. The main interest in this paper is in the region of high energies (HERA and beyond) i.e. sufficiently small \tilde{x} , and small Q^2 , where pQCD contribution dominates because of the rapid increase of the gluon distribution with the decrease of x . The pQCD contribution into the total crosssection initiated by the transverse photon has the form:

$$\begin{aligned} \sigma_T = & 6\pi \frac{\pi\alpha_{\text{e.m.}} \sum e_q^2 F^2}{12} \\ & \times \int_0^1 dz \int dM^2 \alpha_s(4M^2 z(1-z)) \frac{z^2 + (1-z)^2}{z(1-z)} \frac{(M^4 + Q^4)}{(M^2 + Q^2)^4} \cdot g(\tilde{x}, 4M^2 z(1-z)). \end{aligned} \quad (2.7)$$

The invariant mass representation for the transverse photon does not give objective information on the parton transverse momentum distributions. The reason is of course the well known fact, that there are configurations with large invariant masses, but small transverse momenta k_t^2 . These configurations are the perturbative analogues of the AJ configurations. It is useful to rewrite Eq. 2.7 in terms of integration over k_t^2 and z . The reason is that the median invariant mass and transverse momentum for transverse photons are not connected like in the longitudinal photon case, and we need two different equations to determine them. Cross section initiated by the transverse photon has the form:

$$\begin{aligned} \sigma_T = & 6\pi \frac{\pi\alpha_{\text{e.m.}} \sum e_q^2 F^2}{12} \\ & \times \int_0^1 dz \int dk_t^2 \alpha_s(4k_t^2) (z^2 + (1-z)^2) \frac{(k_t^4 + Q^4 z^2 (1-z)^2)}{(k^2 + Q^2 z(1-z))^4} \cdot g(\tilde{x}, 4k_t^2). \end{aligned} \quad (2.8)$$

We include a contribution of the aligned jet configurations by imposing a cut off in transverse momenta. In particular, in the numerical calculations using Eq. 2.8 we introduced a cutoff in the space transverse momenta $k_t^2 = M^2 z(1-z) \geq u$, $u \sim 0.35 \text{ GeV}^2$. The contribution of smaller k_t^2 in the total crosssection was calculated using the AJM model.

III. THE DOUBLE LOGARITHMIC APPROXIMATION.

In this section we analyze the new properties of the pQCD regime within the double log approximation. The advantage of this approximation is that it will allow us to perform some of the calculations analytically. Other calculations will be made numerically but using the expressions that are known analytically.

In the double logarithmic approximation the structure functions are given by [23]

$$xG(x, Q^2) = \int dj / (2\pi i) (x/x_0)^{j-1} (Q^2/Q_0^2)^{\gamma(j)}, \quad (3.1)$$

where the anomalous dimension is

$$\gamma(j) = \frac{\alpha_s N_c}{\pi(j-1)}.$$

To simplify the calculation we assume, the initial condition for the evolution with Q^2 :

$$G(x, Q_0^2) = \delta(x-1). \quad (3.2)$$

In the saddle point approximation one finds [23]:

$$xG(x, Q^2) = \frac{\log(Q^2/Q_0^2)^{1/4}}{\log(x_0/x)^{3/4}} \exp \sqrt{4\alpha_s(Q_0^2)(N_c/\pi) \log(Q^2/Q_0^2) \log(x_0/x)}. \quad (3.3)$$

Structure function of a hadron is given by the convolution of this kernel with the nonperturbative structure function of a hadron in the normalization point $Q^2 = Q_0^2$. Note that G

is increasing with Q^2 . This is the pQCD contribution where virtualities of exchanged gluons are large.

In the analysis of energy dependence of the parton momenta it is legitimate to neglect the pre-exponential factor, since the absolute value of G as well as the pre-exponential factor weakly influence the transverse scale, and its evolution with energy:

$$xG(x, Q^2) = \exp \sqrt{4\alpha_s(Q_0^2)N_c/\pi \log(Q^2/Q_0^2) \log(x_0/x)}. \quad (3.4)$$

We shall consider here the double logarithmic approximation without the running coupling constant. Taking into account the running coupling constant leads to similar results. We shall not present them here, since they are more cumbersome, and are essentially reproduced when we shall tackle the full LO calculations in the next section.

A. Energy dependence of the quark transverse momenta for fragmentation processes initiated by longitudinal photon.

We shall find analytically the scale of the transverse momenta in the limit where $s \gg M^2 \gg Q^2$. For certainty we restrict ourselves to the contribution of light quarks.

At large Q^2 the crosssection for the scattering of the longitudinal photon is dominated by the contribution of the spatially small dipoles, so it is legitimate to neglect the quark masses. In this limit the cross section is proportional to

$$\sigma_L \propto Q^2 \int dM^2 n(M^2, s, Q^2), \quad (3.5)$$

where the function $n(M^2, s, Q^2)$ is given by Eqs. 2.5, 2.6:

$$\begin{aligned} n(M^2, s, Q^2) &= \alpha_s(M^2/4) \frac{M^2}{(M^2 + Q^2)^4} \\ &\times \exp(\sqrt{4\alpha_s(Q_0^2)(N_c/\pi) \log(M^2/Q_0^2) \log((x_0 s)/(M^2 + Q^2))}), \end{aligned} \quad (3.6)$$

where $x_0 = Q^2/s_0$. Here we keep only large terms depending on M^2 (we ignore the M^2 independent normalization factor irrelevant for the calculations below).

Let us show that the maximum of $n(M^2, s, Q^2)$ increases with the energy. At very high energies n is proportional to

$$\begin{aligned} n &\sim \exp(\log \alpha_s(M^2/4) + \log(M^2/Q^2) - 4 \log((Q^2 + M^2)/Q^2)) \\ &+ \sqrt{4\alpha_s(N_c/\pi)(\log(s/s_0) - \log((Q^2 + M^2)/Q_0^2)) \log(M^2/Q_0^2)}. \end{aligned} \quad (3.7)$$

In the limit of fixed Q^2 but very large energies, $\log(s/s_0) \gg \log((Q^2 + M^2)/Q_0^2)$. Let us assume that for the maximum: $M^2 \gg Q^2$. The maximum of the expression 3.7 under this

assumption can be found analytically. We shall see that this assumption is indeed self-consistent. Indeed, under the latter assumption we can differentiate Eq. 3.7 over M^2 and find for the maximum:

$$M^2 = M_0^2 (s/s_0)^{\alpha_s(N_c/\pi)/9}. \quad (3.8)$$

Here $Q_0^2 \sim Q^2$ and $s_0 \sim Q^2$. We will refer to this extremum value of M^2 as M_1^2 . We see from Eq. 3.8 that the condition $M_1^2 \gg Q^2$ is self-consistent at very high energies.

At the extremum $n \propto (\alpha_s(M_1^2/4)/M_1^6 \exp((N_c/\pi)(\alpha_s/3) \log(s/s_0)))$. Therefore

$$\frac{d\sigma_L}{dM^2} \big|_{M^2=M_1^2} \approx \alpha_s(M_1^2/4)(Q^2/M_1^6)(\exp((N_c/\pi)(\alpha_s(Q_0^2)/3) \log(s/s_0))) \quad (3.9)$$

However, the position of the maximum of the integrand is not sufficient to characterize the relevant transverse scales as a large range of M^2 is important in the integrand. In particular, calculation of second derivative shows that dispersion over $M^2 = M_1^2$ is large. The width of the distribution over $\log(M^2/M_0^2)$ is $\sqrt{2/3} \log(M_1^2/M_0^2)$.

Hence we need to determine M^2 range which gives most of the integrand support. For certainty, we define the range of $M^2 \leq M_t^2$ which provides a fixed, say, 50% fraction of the total perturbative cross section. Let us estimate how this scale increases with the energy in the double log approximation. First, let us consider the total cross section. The upper limit u of integration over M^2 is determined by the kinematic condition through t_{\min} , giving that the allowed invariant masses $M^2 \ll s$. We choose upper limit of integration as

$$M^2 \leq M_{max}^2 = 0.2s, \quad (3.10)$$

from the cross section of diffraction although the result of numerical calculations is insensitive to the upper bound because essential M^2 are significantly smaller. In fact the integral for the cross section converges long before the upper limit of integration 3.10 is reached (see the discussion below).

Let us first calculate the median scale semi analytically. Within the double logarithmic approximation, and assuming that the conditions $\log(s/s_0) \gg \log((Q^2 + M^2)/(Q^2 + M_0^2))$, is still valid for the relevant M^2 , the integral for the cross section can be written as:

$$\begin{aligned} \sigma(u) = & (Q^2/Q_0^4) \int_0^{\log(u/M_0^2)} d \log(M^2/Q_0^2) \alpha_s(M^2/4) \exp(-2 \ln(M^2/Q_0^2) \\ & + \sqrt{(4\alpha_s N_c/\pi) \log(M^2/Q_0^2) \log(s/s_0)}). \end{aligned} \quad (3.11)$$

Here u is the upper cut-off in the invariant masses. Introducing the new variable $t = \log(M^2/Q_0^2)$, we obtain:

$$\sigma(u) = (Q^2/M_0^4) \int_0^{\kappa(u)} dt \alpha_s(tM_0^2/4) \exp(-2t + \sqrt{(4\alpha_s N_c/\pi) \log(s/s_0)t}), \quad (3.12)$$

where $\kappa(u) = \log(u/s_0)$. The integral for the total cross section is given by the equation similar to Eq. 3.12, with the upper integration limit being replaced by $\kappa(s) = \sqrt{\log(0.2s/s_0)}$. Note that the essential scale of integration is determined by exponent, and is very weakly influenced by the exact value of a upper cut-off. The integral 3.12 is actually the error

function [24], which can be easily evaluated numerically. Requiring that it gives one half of the cross section we find

$$M_t^2 \sim Q_0^2 (s/s_0)^{0.28\alpha_s N_c/\pi}. \quad (3.13)$$

Evidently, for sufficiently large s our initial assumption $\log(M^2/Q_0^2) \gg \log(Q^2/Q_0^2)$ is fully self-consistent. This is because the decrease of n with M^2 due to $1/M^6$ terms in the integrand of Eq. 2.5 is partially compensated by the rising exponential, giving a relatively slow decrease of n to the right of the maximum of the integrand.

Note that the rate of the increase of M_t^2 with s is much higher than for M_1^2 due to the slow decrease of the integrand with M^2 . The cross section of jet production with M^2 at this interval also increases with the energy as

$$\frac{d\sigma}{dM^2} \Big|_{M^2=M_T^2} \sim (s/s_0)^{0.24\alpha_s N_c/\pi}. \quad (3.14)$$

The analytical calculations supply the pattern for the behavior of the transverse momenta in double log approximation. In order to understand the dependence of the median scale on both the energy and Q^2 quantitatively in the double logarithmic approximation we made numerical calculation of the characteristic transverse momenta using the DGLAP double log structure function. We find that the increase rate of the transverse momenta indeed does not depend on the external virtuality Q^2 . Considering the wide interval of energies and $s = 10^4 \div 10^{11}$ GeV², and $20 < Q^2 < 200$ GeV² we obtain the approximate formulae:

$$M_t^2(x) \sim 0.7Q^2 \exp(0.17((4\alpha_s N_c/\pi) \log(x_0/x))^{0.55}). \quad (3.15)$$

Here $x_0 = 0.01$. We present this estimate only for illustrative purposes, since the double logarithmic approximation is semirealistic only. Still our results indicate that for external virtualities $Q^2 < 100$ GeV² and energies which can be reached at LHeC the onset of a new pQCD regime may take place.

The cross section of the jet production at this scale also increases with the energy as

$$\frac{d\sigma}{dM^2} \Big|_{M^2=M_t^2} \sim (G(x, Q^2)/Q^6)(M_t^2(x)) \quad (3.16)$$

where $M_t^2(x)$ is given by Eq. 3.15. The median transverse momenta $k_t^2 \sim M_t^2/4$, due to the dominance of symmetric configurations.

B. Transverse photon: the characteristic transverse scale in the photon fragmentation region.

The main difference between the longitudinal and transverse structure functions in the DIS is the presence of the strongly asymmetrical in z configurations due to the presence of the $(z(1-z))^{-1}$ factor in the spectral density. As a result there is a competition between two effects. One is a slower decrease of the spectral function with M^2 (by the factor M^2/Q^2), leading to the more rapid increase of the characteristic transverse momenta for the symmetric configurations. Another effect is the presence of the asymmetric ($z \rightarrow 0$) configurations which are characterized by the small transverse momenta k_t^2 for a given invariant mass M^2 . For such configurations the rate of increase of the gluon structure function with energy is small.

Let us first show that the transverse momenta increase rapidly for symmetric configurations. The spectral representation for the transverse photon for symmetric configurations is proportional to

$$n(M^2, Q^2, s) \sim \frac{M^4 + Q^4}{(M^2 + Q^2)^4} \times \sqrt{4\alpha_s(N_c/\pi)(\log(s/s_0) - \log((Q^2 + M^2)/(Q_0^2)) \log(M^2/Q_0^2))}. \quad (3.17)$$

In the high energy limit, when $M_1^2 \gg Q^2$, we find for the dependence of the maximum of n on energy:

$$M_1^2 \sim Q_0^2(s/s_0)^{\alpha_s(N_c/\pi)/4}. \quad (3.18)$$

This is twice as fast increase as for the case of the longitudinal photon. M_1^2 increases with s at high energies and thus the condition $M^2 \gg Q^2$ is perfectly self-consistent at very high energies. In addition we can calculate the total cross section in the same approximation semi-analytically getting the error function and obtain the rate of increase $(s/s_0)^{0.14(4\alpha_s N_c/\pi)}$, which is twice that for the longitudinal case.

These two results are applicable to the symmetric configurations only. On the other hand, at least at achievable energies, the dominant contributions for transverse photon crosssection are asymmetric, with z close to 0 or 1. In order to take these configurations into account we performed a numerical calculation using the gluon distribution function within the double log approximation. The result is that the characteristic median scale M_t^2 increases as

$$M_t^2 \sim M^2(Q^2)(s/s_0)^{0.1(4\alpha_s N_c/\pi)}. \quad (3.19)$$

The value of the exponent is 0.12 for the beginning of the studied energy range $s \sim 10^4 \div 10^{11}$ GeV², and decreases to 0.09 at the upper end (for typical $\alpha_s = 0.25$). Thus the rate of the increase with the energy is approximately the same as for longitudinal photons for not very high energies. For very high energies the symmetric configurations win over asymmetric ones, leading to the increase of the average transverse momentum squared which is twice as large as in the longitudinal case. The precise determination of the scale $M_0^2(Q^2)$ is beyond the accuracy of this approximation. Effectively we obtain the dependence $M_t^2 \sim 0.7Q^2(x_0/x)^{0.1(4\alpha_s N_c/\pi)}$.

One can also estimate the rate of the increase of the jet production cross section :

$$d\sigma_T/dM_{M_t^2}^2 \sim (xG(x, Q^2)/Q^4)(1/3)(1 + 0.5(x_0/x)^{0.24}). \quad (3.20)$$

We found a rapid increase of the jets multiplicity with energy. Thus the rate of the increase with energy of the transverse momenta of quarks in the current fragmentation region for transversely polarized photon is significantly more rapid. Consequently we find that $\sigma_L/\sigma_T \approx \alpha_s Q^2/M^2$ being numerically small should slowly decrease with energy at sufficiently high energies .

We conclude that it is possible to show analytically that for very high (asymptotic) energies the relevant invariant masses extend well beyond Q^2 and increase with the energy. The direct numerical calculation of the M_t^2 scale shows that the rate of increase is independent of external virtuality.

Note that due to the significant contribution of the asymmetric configurations the median transverse momenta is much smaller than $M_t^2/4$. The simple numerical calculations using $k_t^2 = M^2 z(1-z)$, shows that the average transverse momenta (including nonsymmetric configurations) rapidly increases like $a(Q^2)/(x/0.01)^{0.12}$, with the exponent once again is independent of external virtuality, and $a(Q^2) \sim 0.6\text{GeV}^2 + 0.02Q^2$, i.e. k_t^2 is much smaller than $M^2/4$, especially for small virtualities.

IV. THE CHARACTERISTIC TRANSVERSE MOMENTA IN HARD FRAGMENTATION PROCESSES IN LO APPROXIMATION.

In the previous section we discussed the quantitative dependence of the characteristic transverse scales of DIS in the double logarithmic approximation in the dipole model at unrealistically high energies, where the analytical calculations are possible. Here we carry out the calculations for realistic energies and realistic structure functions. The numerical results indicate that the effects discussed above are manifest even at the energies of the order $s \sim 10^5 \div 10^6 \text{ GeV}^2$.

We will also consider the extrapolation of our results to energies of the order $s \sim 10^7 \text{ GeV}^2$. These energies are unattainable at existing facilities. The proposed LHeC collider may reach the invariant energies of order 10^6 GeV^2 [25]. However these results are interesting from the theoretical point of view- probing the limits of the pQCD.

The challenging and unresolved problem is how to use resummation methods at extremely small x [26, 27] to evaluate dependence on energy of parton distribution in the current fragmentation region. One can substantiate this point by evaluation of the number of radiated gluons in the multiRegge kinematics [15], obtaining 1-2 emissions at HERA energies. However at extremely small x where number of gluon radiations would be sufficiently large and therefore these models can become applicable. This interesting problem is beyond the scope of this paper.

A. The longitudinal photons.

In the case of longitudinal photons we have considered the characteristic median/average transverse momenta scale, that corresponds to the half of the total crosssection σ_L . This scale is determined from Eq. 2.5 by first integrating over z for given k_t , and then analyzing the corresponding jet distribution. The results of the numerical analysis using the CTEQ6 gluon distribution functions are given in the Table 1. In Figure1 we present the characteristic graphs for the ratio

$$R(k_t^2) = \frac{\sigma(k_t^2)}{\sigma_L}, \quad (4.1)$$

where $\sigma(k_t^2)$ corresponds to the result of integration of Eq.2.6 over transverse momenta $\leq k_t^2$. We see from Fig. 1, that for fixed k_t $R(k_t)$ slowly increases with the increase of the energy. The results based on using CTEQ5 parametrization are qualitatively similar, although the increase of median k_t^2 with the energy is more rapid. The energy dependence of median k_t^2 can be described with a very good accuracy by an approximate formula $(x/0.01)^{0.04+0.025 \log(Q^2/Q_0^2)}$. Here $Q_0^2 = 10 \text{ GeV}^2, x_0 \sim 0.01$. The power increases from ~ 0.04 at $Q^2 \sim 5 \text{ GeV}^2$, to 0.09 at $Q^2 \sim 100 \text{ GeV}^2$. The interpolation expression which provides a good description of the results presented in Table 1 is given in Appendix E. For CTEQ5 the

exponent in Eq. E1 increases to 0.1 at $Q^2 = 100 \text{ GeV}^2$ instead of 0.09. This is consistent with the enhanced rate of the increase of CTEQ5 structure functions as compared to the CTEQ6 ones (see below).

These results allow us to estimate the scales, where one expects the appearance of the new QCD regime, i.e. one has to use the k_t factorization approach. Indeed, the DGLAP approximation is based on the strong ordering in all rungs of the ladder, in particular in the first rung (the impact factor in the $4k_t$ factorization language) we must have $4\Lambda_{\text{QCD}}^2 \leq 4k_t^2 \leq Q^2$. It is clear, this ordering can not hold, once the median $4k_t^2$ becomes of order Q^2 . Then we obtain the condition (using CTEQ6 distribution functions):

$$4a(Q^2)/(x/0.01)^{0.04+0.025 \log(Q^2/Q_0^2)} \sim Q^2. \quad (4.2)$$

Here the function a corresponds to the transverse momenta at $x = 0.01$.

The analysis of Table 1 and Fig.1 shows that for $Q^2 = 5 \text{ GeV}^2$ one gets from eq. 4.2 $x \sim 10^{-4}$, for $Q^2 = 10 \text{ GeV}^2$ one gets $x \sim 10^{-6}$, which may be reached at LHeC. For larger Q^2 we are however beyond the realistic energies: say for $Q^2 \sim 20 \text{ GeV}^2$ we need $x \sim 10^{-9}$. The use of CTEQ5 gives qualitatively the same results (for $Q^2 = 30 \text{ GeV}^2$ we obtain $x \sim 10^{-8}$). Thus we may hope to observe the onset of the new regime for the k_t dependence analyzing small x jet distributions at LHeC/LHC.

The similar analysis can be made using Eq. 2.5 and considering the invariant masses M^2 . We obtain that our results for median invariant masses are $M^2 \sim (4 \div 5)k_t^2$, confirming the dominance of the symmetric configurations.

B. Transverse photons.

We perform the numerical analysis for the transverse photons using eqs. 2.7,2.8 in the same fashion as for the longitudinal photons. The results for the median transverse momenta are given in Table 2. In figure 2 we depicted the characteristic function $R(k_t^2)$ given by Eq. 4.1 that gives the characteristic momenta as a function of x for typical value of $Q^2 = 40 \text{ GeV}^2$. The characteristic energy dependence in Table 2 for median k_t^2 is $(x/0.01)^{0.09+0.014 \log(Q^2/Q_0^2)}$ where $x_0 = 0.01, Q_0^2 = 10 \text{ GeV}^2$. A complete expression is given in appendix E. The curves in Fig. 2 clearly show that the characteristic momenta increase with the increase of $1/x$, as the corresponding curves slowly shift to the right.

We see from the Table 2 that the average transverse momenta for longitudinal photons is significantly larger than for transverse photons. On the other hand, the invariant masses for transverse photons are always significantly larger than $4k_t^2$. This is due to the large contribution of the AJM type configurations with $z \sim 0, 1$. Since $M^2 = k_t^2/(z(1-z))$, a more slow increase of M^2 than of k_t^2 is consistent with the slow increase of average z towards $1/2$, i.e. the symmetric configurations become dominant, but only at asymptotically large energies.

Once again, we can estimate the boundary of the region where the direct DGLAP approach stops being self-consistent. Assuming $k_t^2 \sim Q^2/4$, we obtain that the boundary for $Q^2 = 3, 5, 10 \text{ GeV}^2$ is reached at $x \sim 10^{-3}, 10^{-4}, 10^{-6}$. For higher Q^2 this boundary lies at unrealistically high energies. The use of the CTEQ5 parametrization gives qualitatively the same results.

So far we considered only perturbative QCD contribution, and the median transverse momentum in Table 2 is determined relative to the total perturbative cross section, i.e. the

one starting from the cut off $u = 0.35 \text{ GeV}^2$. However, as we mentioned above, there is also important AJ contribution in a total cross section. In this paper we take them into account using the AJM model [30] (see also Appendix B). This contribution is given in Table 3. It is well known that at low x AJM gives a dominant contribution into cross section. For $x \sim 0.01$, $Q^2 \sim 1 \text{ GeV}^2$ we see from Table 3 that AJM gives 70% of the total cross section. However even at HERA energies the contribution of AJM into the total cross section remains significant. Note that the median k_t^2 at small virtualities at HERA energies significantly decreases if we calculate it using the cross section that includes both the pQCD and soft (AJM) contributions. For example, at $Q^2 \sim 10 \text{ GeV}^2$ the median transverse momentum squared decreases by almost a factor of two down to $k_t^2 \sim 0.65 \text{ GeV}^2$.

V. DEEPLY VIRTUAL COMPTON SCATTERING.

As the application of the formulae obtained in this paper we shall consider the DVCS processes $\gamma + p \rightarrow \gamma^* + p$. We shall show that the slow increase in the median transverse momenta leads to the slow decrease of the ratio $R = A_{\text{DVCS}}/A_{\text{CS}}$ with energy to the limiting value equal one.

The DCVS amplitude is described in pQCD by the same formula 2.7 as the amplitude describing total cross section of DIS at given x, Q^2 but with the substitution in Eq.2.3 of the wave function of virtual photon by wave function of a real photon, i.e. $Q^2 = 0$.

As a result in pQCD R has the form :

$$R_{\text{pQCD}} = \frac{\int_0^1 dz \int dM^2 \alpha_s(M^2 z(1-z)) (1/(M^2 + Q^2)^2) \cdot g(\tilde{x}, M^2)}{\int_0^1 dz \int dM^2 \alpha_s(M^2 z(1-z)) ((M^4 + Q^4)/(M^2 + Q^2)^4) \cdot g(\tilde{x}, M^2)}. \quad (5.1)$$

Let us note that strictly speaking, we must use the generalized parton distributions (GPD) in Eq. 5.1. However the difference between gluon GPD and gluon pdf is not large in this case because fractions carried by gluons in GPD differ by the factor \approx two at moderate x and tend to one at extremely large energies as the consequence of increase of parton momenta with energy. (In fact most of the non-diagonal effect in this approach is included in the wave functions of the initial and final photons.) Indeed, the DVCS amplitude is expressed in terms of gluon GPD where $x_1 = M^2/s, x_2 = (M^2 + Q^2)/s$. Our analysis above shows that $M^2 \approx Q^2$ at moderate energies. So $x_1 \approx x \approx x_2/2$. Analysis of the QCD evolution equation for GPD [28] shows that $x_1 G(Q^2, x_1, x_2) = g(Q^2, x_1, x_2) \approx g(Q^2, (x_1 + x_2)/2) = g(Q^2, 1.5x)$. At small x $g(Q^2, 3/2x)/g(Q^2, x) \approx 1/(3/2)^{1/4} \approx 0.9$. In the regime when $M^2 \gg Q^2$ $x_1 \approx x_2$. So GPD coincides with the gluon density. As a result we may neglect the difference between GPD and distribution functions in the considered kinematics. The numerical analysis of Eq. 5.1 shows that the ratio R very slowly decreases with the increase of energy due to a slow increase of a ratio M^2/Q^2 discussed in the previous section, and $R \sim 1.6$ for HERA energies.

The result Eq. 5.1 is however not complete since we neglected the contribution of the AJ configurations. Indeed, we already saw in the previous section (Table 3) that it gives significant contribution in a total cross-section. In the framework of the AJM model the ratio of amplitudes of the DVCS to DIS can be calculated within the leading twist approximation as [29]:

$$R_{\text{AJM}} = \frac{Q^2 + m_0^2}{Q^2} \log(1 + \frac{Q^2}{m_0^2}). \quad (5.2)$$

Here the parameter $m_0^2 = 0.3 - 0.5 \text{ GeV}^2$ is the cut off parameter $m_0^2 \leq m_\rho^2$, m_ρ is the ρ meson mass.

Combining the pQCD and AJ model contributions we have

$$R = \frac{R_{\text{pQCD}}\sigma_T + R_{\text{AJM}}\sigma_{\text{AJM}}}{\sigma_T + \sigma_{\text{AJM}}}. \quad (5.3)$$

Here the pQCD contribution into the total cross section σ_T is given by Eq. 2.7 and the contribution of AJ to the total cross section is given by AJM - Eq. B1. The results of numerical calculation with parameter $m_0^2 \sim 0.5 \text{ GeV}^2$ are given in Table 4. We depict these results as a function of x for several values of Q^2 in Fig 4. The ratio R is close to 2 at HERA energies and increases with Q^2 (from 5 to 100 GeV^2 by $\sim 40\%$). This result is in a good agreement with the analysis of the H1 and ZEUS data in Ref. [31] (see in particular Table 4 in Ref. [31]). Our main prediction is that the ratio R should decrease with the rise of energy. It tends to one at asymptotically large energies in agreement with the result for the BDR [33]. However the onset of this regime is very slow. This prediction can be checked experimentally in the study of DVCS processes at LHeC.

Our conclusion on the important role of AJM contribution in DVCS at HERA energies is in the qualitative agreement with the recent experimental data [32] that shows the important role of soft QCD in the diffractive processes in DIS at HERA.

We want to draw attention that agreement between experimental results and theoretical prediction is rather good. This is due to the fact that the interaction of dipole effectively includes the NLO corrections since parton distributions were obtained by fitting the experimental data. Consequently one may hope that NLO corrections to impact factors are relatively small.

Let us stress that the current calculation is preliminary. More detailed calculation should account for the contribution of c-quark, and study in detail the dependence of R on the AJM parameters).

VI. ON THE INCREASE WITH ENERGY OF PARTON MOMENTA IN THE CURRENT FRAGMENTATION REGION IN THE BLACK DISC LIMIT.

In the previous sections we found the increase with the energy of the parton momenta in the current fragmentation region in the pQCD regime.. Here we shall consider the configurations in the projectile wave function that become dominant just near the transition to the black disk limit. We will explain that due to the dominance of these configurations, the increase with the energy of the parton transverse momenta in the current fragmentation region is further accelerated at the energies where the DGLAP and BFKL approximations to QCD violate conservation of probability/unitarity

The aim of the present chapter is to analyze the properties of this new QCD regime (we also call it the black disk regime; let us stress that this regime is different from the possible new pQCD regime that was discussed in the previous sections). We shall study the increase of the characteristic transverse momenta of the configurations in the wave function of the projectile responsible for the blackening, and derive a expression for the total cross-section. This expression gives a total cross section as a function of a transverse momentum increase rate.

We will use the probability conservation for the amplitude describing the dipole scattering at given impact parameter b . In the kinematics of $x \ll 1$ Feynman amplitude describing scat-

tering of dipole off a target $A(x, t, Q^2)$ is calculable in terms of partial amplitude $f(b^2, x, Q^2)$ as

$$A(x, t = -q_t^2, Q^2) = 2s \int d^2b \exp(i\vec{q}_t \vec{b}) f(b^2, x, Q^2), \quad (6.1)$$

and

$$f(b^2, x, Q^2) = \int \frac{d^2q_t}{8\pi^2} \exp(i\vec{q}_t \vec{b}) \frac{A(x, t, Q^2)}{s}. \quad (6.2)$$

In a quantum theory the elastic cross section for the scattering of dipole off target T is given by the well known formulae :

$$\sigma_{el} = \int d^2b |f(b, x, Q^2)|^2, \quad (6.3)$$

The inelastic cross section is given by:

$$\sigma_{in} = \int d^2b (1 - |1 + if(b^2, x, Q^2)|^2), \quad (6.4)$$

and total cross sections is equal to:

$$\sigma_{tot} = 2 \int d^2b \text{Im} f(b^2, x, Q^2). \quad (6.5)$$

It follows from these equations that

$$\text{Im} f(b^2, x, Q^2) \leq 1. \quad (6.6)$$

The limit

$$\text{Im} f(b^2, x, Q^2) = 1, \quad (6.7)$$

is reached in the small x regime when a small transverse size of the quark-gluon dipole is absorbed by the target with the 100% probability at given b .

In the numerical evaluations it is convenient to use profile function $\text{Im} f = \Gamma$ and neglect $\text{Re} f$ as compared to $\text{Im} f$, which is justified at sufficiently high energies.

These equations allow us to evaluate some important properties of the onset of the new QCD regime of strong interaction with small coupling constant and the kinematical region of applicability of perturbative QCD to hard processes.

- According to Eq.6.2 the dependence of Γ on impact parameter b is given by the Fourier transform of the two gluon form factor of a nucleon. It was measured in the hard exclusive vector meson production at HERA and at FNAL. The two gluon formfactor can be parameterized as: $F(q^2) = 1/(1 + q^2/\mu^2)^2$, with μ decreasing with the decrease of x ($\mu^2(10^{-2}) \sim 1 \text{ GeV}^2$, $\mu^2(10^{-4}) \sim 0.7 \text{ GeV}^2$), cf. discussion in Appendix C. Within the framework of pQCD at large k_t the dependence of μ on x due to Gribov diffusion in the impact parameter space should be a small effect. Variation of μ comes mainly from the diffusion at $Q^2 \sim Q_0^2$ which is moderate, and it is further suppressed by the DGLAP evolution [34]. Thus

$$\Gamma(b, x) = (x_o/x)^{\lambda(4k_t^2)} \mu b K_1(\mu b). \quad (6.8)$$

Here K_1 is the MacDonald function and k_t is the parton transverse momentum within the dipole. Parameter x_o is function of k_t^2 calculable in pQCD. The dependence on energy has been evaluated within pQCD or using the experimental data. Experimentally $\lambda(10 \text{ GeV}^2) \approx 0.2$ and increases with k_t^2 .

- Knowledge of x, b, k_t dependencies of Γ and Eq.6.7 allows us to evaluate the characteristic k_t in the region, where the onset of the black disc regime occurs. This evaluation predicts significantly more rapid increase with energy of k_t in the vicinity of black disc limit than the calculations performed in the preceding sections. This is the signature of the blackening of the interaction, i.e. of the transition to the regime described by Eq.6.7. Since the integration over k_t is logarithmic, it is determined by the upper limit of the integration over k_t^2 in the probability defined by the wave function of the dipole. The dependence of k_t on collision energy is determined as the rate of increase of the black disc momenta squared with energy:

$$k_{tb}^2 \sim k_{tb0}^2 (s/s_0)^\kappa, \quad (6.9)$$

where $s_0 \sim 10^4 \text{ GeV}^2$ (corresponds to the HERA energy). The dependence of k_{tb}^2 on s is depicted in Tables 5,6. Note that κ does not depend on whether we take $\Gamma = 1/2$ or $\Gamma = 1$ as a blackness condition, and is the same for fermionic and gluonic dipoles. Our results show that this coefficient weakly depends on energy, with $\kappa = 0.3 \div 0.4$ at the LHC energies and beyond.

- The slope of t dependence of the cross sections of hard exclusive processes at $t=0$ - $B(0)$

$$B(0) = \frac{\int d^2b b^2 [\Gamma(b^2, x, Q^2)]}{\int d^2b [\Gamma(b, x, Q^2)]}, \quad (6.10)$$

should increase with energy in the vicinity of BDR and at larger energies. This property follows from the increase with energy of the essential impact parameters. Using Eq.6.2 we obtain equation for maximal $b = b_M$ where Γ is equal to 1:

$$1/\log(\mu b_M K_1(\mu b_M)) = \kappa \log(x_0/x). \quad (6.11)$$

At sufficiently large energies where $\kappa \log(x_0/x) \geq 1$ the above equation has the solution:

$$\mu b_M = \kappa \log(x_0/x). \quad (6.12)$$

Evidently $b_M(x \rightarrow 0)$ would become practically independent of x_0 .

Note that within the LT approximation μ and therefore the slope B are slowly increasing with energy in some interval of $x \sim 0.01$ as the consequence of spontaneously broken chiral symmetry. The long range pion cloud carries small fraction $\approx m_\pi/m_p$ of proton momentum and therefore scattering off this cloud is suppressed at not too small x because amplitude is rapidly decreasing with decrease of collision energy [15].

A slightly more sophisticated reasoning which uses the completeness over the hadronic states shows that Eqs.6.11, 6.12 are valid even if we account for the gluons and quark-antiquarks pairs in the wave function of the dipole.

- Knowledge of b_M and Eq.6.5 allows us to calculate the total cross section of the scattering of the spatially small dipole. We have $\Gamma = 1$ for $b \leq b_M$, $\Gamma(b \geq b_M) = b K_1(\mu(x)b)/b_M K_1(\mu(x)b_M)$. Then we have

$$\begin{aligned} \sigma &= 2\pi b_M^2 + 2 \int d^2b \Theta(b - b_M) \Gamma(b, x, Q^2) \\ &= 2\pi(b_M^2 + 2(b_M/\mu) K_2(b_M\mu)/K_1(b_M\mu)). \end{aligned} \quad (6.13)$$

Here to calculate the second integral we use an identity between special functions:

$$\frac{d}{dx}(x^2 K_2(x)) = -x^2 K_1(x)$$

The second term in the second line of eq. 6.13 is the contribution of peripheral collisions. Thus cross sections of hard processes integrated over impact parameters would increase with energy forever.

Note that using eq. 6.13 we can estimate, what part of the total cross section comes from the black disk regime, and what part from pQCD. Indeed, estimating b_M as a scale at which the black transverse momentum is of order ~ 1 GeV, we have $b_M \sim 4.5$ GeV⁻¹ for typical $x \sim 10^{-6}$, $Q^2 \sim 10$ GeV². We use a typical value of $\mu \sim 0.7$ GeV for these energies. Then the contributions of black disk to total cross section is of the order 66%. Let us stress that here we assume $b_M \ll 1/(2m_\pi)$ which is a typical scale for the phenomenon of spontaneously broken chiral symmetry in the soft QCD physics.

VII. THE COHERENCE LENGTH AND THE SHAPE OF THE FAST NUCLEON AND NUCLEI.

A. The coherence length.

In the previous sections we determined the energy dependence of the effective transverse scale at high energies. This result allows us to evaluate the coherence length. The coherence length l_c corresponds to the life-time of the dipole fluctuation at a given energy in the rest frame of the target. The original suggestion of the existence of the coherence length in the deep inelastic scattering was first made by Ioffe, Gribov and Pommeranchuk [21, 35]. It was found already in the sixties within the parton model approximation by Ioffe [36] that the coherence length at moderate x is $l_c \sim 1/2m_N x$ i.e. it linearly increases with energy. In the pQCD as a result of QCD evolution coherence length increases with energy more slowly:

$$l_c = (1/2m_N x)(s_0/s)^\lambda. \quad (7.1)$$

Such a behavior of l_c with energy has been found previously in the numerical calculations of structure functions in the target rest frame [37, 38, 39].

In a similar way, once we have the onset of the black limit regime, the coherence length corresponding to the dominant configurations in the process decreases even more slowly:

$$l_c = (1/2m_N x)(s_0/s)^\kappa. \quad (7.2)$$

Here κ is the rate of the increase of the black disk transverse momenta, given by eq. 6.9.

B. The shapes of the fast nucleons and nucleus.

The results from the previous subsection have the important consequences for the transverse structure of the hadrons and nuclei.

Let us consider the longitudinal distribution of the partons in a fast hadron. In the parton model the longitudinal spread of the gluonic cloud is $L_z \sim 1/\mu$ for the wee partons (where

$\mu \sim 0.3 \div 0.4 \text{ GeV}/c$ is the mass scale of soft QCD processes.) and it is much larger than for harder partons, with $L_z \sim 1/xP_h$ for partons carrying a finite x fraction of the hadron momentum [10]. The picture is changed qualitatively in the limit of very high energies when interactions reach BD regime for $k_t \gg \mu$. In this case the smallest possible characteristic momenta in the frame where hadron is fast are of the order $k_t(BDR)$ which is a function of both initial energy and transverse coordinate, b of the hadron. Correspondingly, the longitudinal size is $\sim 1/k_t(BDR) \ll 1/\mu$. Note here that we are discussing longitudinal distribution for typical partons. There is always a tail to the momenta much smaller than typical all the way down to $k_t \sim \mu$ which corresponds to the partons with much larger longitudinal size (a pancake of soft gluons corresponding to the Gribov's picture). However at large energies at the proximity of the unitarity limit the contribution of the gluons with $k_t < k_{tb}$ is strongly suppressed [40]. In the BDR this tail is suppressed by a factor $k_t^2/k_t(BDR)^2$ in addition to the phase factor [14]. In the color glass condensate model the suppression is exponential [41].

Since the gluon parton density decreases with the increase of b the longitudinal size of the hadron is larger for large b , so a hadron has a shape of biconcave lens, see Figs. 5,6.

In the numerical calculation we took

$$|l_z| = 1/k_t(BDR), \quad (7.3)$$

neglecting overall factors of the order of one (typically in the Fourier transform one finds $\langle z \rangle \sim \frac{\pi}{\langle p_z \rangle}$). We calculated $k_t(BDR)$ for fixed external virtuality $Q^2 \sim 40 \text{ GeV}^2$. Our results are not sensitive to the value of Q_0^2 , as the value of Q^2 only enters in the combination $x' = (Q^2 + M^2)/s$, and the k_t^2 we found were comparable or larger than $Q^2/4$. Indeed, the direct calculation shows that for small b the change of $1/k_t$ if we go between external virtualities of 60 and 5 GeV^2 is less than 5%. Such weak dependence continues almost to the boundary of the picture 5 where $k_t \sim 1 \text{ GeV}$. Near the boundary the uncertainty increase to $\sim 25\%$, meaning that for large b (beyond those depicted in Fig. 5) the nucleon once again becomes a pancake and there is a smooth transition between two pictures (biconcave lens and pancake). We want to emphasize here that the discussed above weak dependence of $k_t(BDR)$ on the resolution scale indicates that the shape of the wave function for small x is almost insensitive to the scale of the probe.

We depict the typical transverse quark structure of the fast nucleon in Fig. 5. We see that it is drastically different from the naive picture of a fast moving nucleon as a flat narrow disk with small constant thickness. (Similar plot for the gluon distribution is even more narrow). Note also that for the discussed small x range $k_t \geq 1 \text{ GeV}/c$ for $b \leq 1 \text{ fm}$. Since the spontaneous chiral symmetry breaking corresponds to quark virtuality $\mu^2 \leq 1 \text{ GeV}^2$, probably $\sim 0.7 \text{ GeV}^2$ [42], corresponding to $k_t \sim \sqrt{\frac{2}{3}}\mu^2 \sim 0.7 \text{ GeV}/c$ the chiral symmetry should be restored for a large range of b in the proton wave function for small x .

Let us consider the case of the DIS on the nuclei. First, we consider the case of external virtualities of the order of several GeV . In this case the shadowing effects to the large extent cancel the factor $A^{1/3}$ in the gluon density of a nucleus for the central impact parameters, b [43], and the gluon density in the nuclei is comparable to that in a single nucleon for $b \sim 0$. Consequently over the large range of the impact parameters the nucleus longitudinal size is approximately the same as in the nucleon at $b \sim 0$.

However for very small x we find large $k_t(BDR)$ corresponding to $4k_t^2(BDR) \geq 40 \text{ GeV}^2$. This is a self consistent value as indeed for such Q^2 the leading twist shadowing is small. Accordingly we calculated the shape of the nucleus for the external virtuality $Q^2 \geq 40 \text{ GeV}^2$.

We should emphasize here that taking a smaller virtuality would not significantly change our result for $k_t(BDR)$ (at the same time LT nuclear shadowing reduces a low momentum tail of the k_t distribution as compared to the nucleon case). In the discussed limit of the small leading twist shadowing, the corresponding gluon density unintegrated over b is given by a product of a nucleon gluon density and the nuclear profile function:

$$T(b) = \int dz \rho(b, z), \quad (7.4)$$

where the nuclear three-dimensional density is normalized to A . We use standard Fermi step parametrization [44]

$$\rho(r) = C(A) \frac{A}{1 + \exp((r - R_A)/a)}, \quad R_A = 1.1A^{1/3} \text{fm}, a = 0.56 \text{fm}. \quad (7.5)$$

Here $r = \sqrt{z^2 + b^2}$, and A is the atomic number. $C(A)$ is a normalization factor, that can be calculated numerically from the condition $\int d^3r \rho(r) = A$. At the zero impact parameter $T(b) \approx 0.5A^{1/3}$ for large A .

The dependence of the thickness of a fast nucleus as a function of the transverse size is depicted in Fig. 6 for a typical high energy $s = 10^7 \text{ GeV}^2$, $Q^2 = 40 \text{ GeV}^2$. We see that the nuclei also has a form of a biconcave lens instead of a flat disk. The dependence on the external virtuality for the nuclei is qualitatively very similar to the case of the nucleon. For small b the dependence is very weak (of order 5%) and increases only close to the boundary of the biconcave lens region where it is of order 20% (and $k_t \sim 1 \text{ GeV}$). For larger b we smoothly return to the pancake picture.

Note that this picture is very counterintuitive: the thickness of a nucleus is smaller than of a nucleon in spite of $\sim A^{1/3}$ nucleons at the same impact parameter. The resolution of the paradox in the BD regime is quite simple: the soft fields of individual nucleons destructively interfere cancelling each other. Besides for a given impact parameter b , the longitudinal size of a heavy nucleus $1/k_t^{(A)}(BDR) < 1/k_t^{(p)}(BDR)$ since the gluon distribution function in the nuclei $G_A(x, b) > G_N(x, b)$. So a naive classical picture of a system build of the constituents being larger than each of the constituents is grossly violated. The higher density of partons leads to the restoration of the chiral symmetry in a broad b range and much larger x range than in the nucleon case.

VIII. EXPERIMENTAL CONSEQUENCES.

The current calculations of the cross sections of the hard processes at the LHC are based on the use of the DGLAP parton distributions and the application of the factorization theorem. Our results imply that the further analysis is needed to define the kinematic regions where one can use DGLAP distributions. We showed in the paper that for DIS at high energies in the kinematical region of sufficiently small x it is necessary to use the k_t factorization and the dipole model, instead of the direct use of DGLAP.

A similar analysis must be made for the pp collisions at LHC. It has been understood long ago that the probability of pp collisions at central impact parameter is close to 100% (total Γ is close to 1) even for soft QCD, i.e. at lesser energies than those necessary to achieve BDR for the hard interactions. The compatibility of probability conservation with the rapid increase of hard interactions with energy, predicted by QCD, requires the decrease of importance of

soft QCD contribution with energy [45]. As a result the hadronic state emerged in pp, pA, AA collisions at sufficiently large energies consists of two phases. Central collisions would be dominated by the strong interaction with small coupling constant - the phase with unbroken chiral and conformal symmetries. On the contrary, the peripheral collisions are dominated by the more familiar phase with broken chiral and conformal symmetries. At these energies the QCD phase at central collisions - with the unbroken chiral and conformal symmetries - will be different from that for the peripheral collisions. This new phenomena may appear especially important for the central heavy ion collisions at LHC and at RHIC. Quantitative analysis of this problem will be presented elsewhere.

The hard processes initiated by the real photon can be directly observed in the ultraperipheral collisions [46]. The processes where a real photon scatters on a target, and creates two jets with an invariant mass M^2 , can be analyzed in the dipole model by formally putting $Q^2 = 0$, while M^2 is an invariant mass of the jets. In this case with a good accuracy the spectral density discussed above will give the spectrum of jets in the fragmentation region. Our results show that the jet distribution over the transverse momenta will be broad with the maximum moving towards larger transverse momenta with increase of the energy and centrality of the γA collision.

We have seen that our results can also describe DCVS processes. The ratio R of DCVS $\gamma^* \rightarrow \gamma^*$ and forward amplitudes at $t = 0$ is of order 2 at HERA energies at small external virtualities, and rapidly growing with Q^2 . This ratio slowly decreases with the decrease of x .

Finally, our results can be checked directly, if and when the LHeC facility will be built at CERN. One of us, B.Blok, thanks S.Brodsky for the useful discussions of the results obtained in the paper. This work was supported in part by the US DOE Contract Number DE- FG02-93ER40771 and BSF.

APPENDIX A: THE BASICS OF THE DIPOLE APPROXIMATION APPROACH.

The QCD factorization theorem allows to express the total cross section of the DIS off a hadron through the convolution of the virtual photon wave function. LO approximation is equivalent to the dipole approximation and the cross section of the dipole scattering off a hadron [19].

In this section we shall remind the reader the basic idea of the derivation of this result [19, 20]. Consider for the simplicity the case of the longitudinal photon. The total cross section of the photon scattering off the target T has the following factorized form:

$$\sigma = \int \frac{d^4 k}{(2\pi)^4} \frac{1}{s(k^2)^2} (2\text{Im} T_{\mu\nu}^{abN}) (\text{Im} T_{\bar{\mu}\bar{\nu}}^{ab}) d_{\mu\bar{\mu}} d_{\nu\bar{\nu}}. \quad (\text{A1})$$

Here $d_{\mu\bar{\mu}}/k^2$ is the propagator of the exchanged gluon in the light-cone gauge, TT is the sum of the box diagrams describing the scattering $\gamma^* g \rightarrow \bar{q}q$, and T is the amplitude of the gluon scattering of the target. Restricting ourselves to the contribution of longitudinal gluon [47] polarization and using the Sudakoff decomposition, the latter equation can be rewritten as

$$\sigma = \int \frac{d\alpha d\beta d^2 k_t}{8(pq)^2 (2\pi)^4 (k_t^2)^2} (\text{Im} N_{\mu\nu}^{ab} p^\mu p^\nu) (\text{Im} T_{\bar{\mu}\bar{\nu}}^{ab} q^{\bar{\mu}} q^{\bar{\nu}}). \quad (\text{A2})$$

Using the Ward identity we can rewrite:

$$\frac{\text{Im} N_{\mu\nu}^{ab} p^\mu p^\nu}{4(pq)^2} = \frac{\text{Im} N_{\mu_t\nu_t}^{ab} k^{\mu_t} k^{\nu_t}}{(\beta s)^2}. \quad (\text{A3})$$

Since we integrate over $d^2 k_t$, the r.h.s. of Eq. A3 can be substituted by $\sum_{\mu_t=1,2} \text{Im} N_{\mu_t\nu_t}^{ab} k_t^2$. The latter term can be directly connected with the scattering cross section $\gamma^* g \rightarrow \bar{q}q$:

$$\delta_{ab}(\beta s - Q^2) \sigma(\gamma^* g \rightarrow \bar{q}q) = \frac{1}{2} \sum_{\mu_t\nu_t} \text{Im} N_{\mu_t\nu_t}^{ab} \quad (\text{A4})$$

Here α, β are the Sudakoff parameters of the gluon momenta k :

$$k = -\alpha q' + \beta p' + k_t, \quad (\text{A5})$$

q is the photon and p is the target momenta. The total cross section then can be rewritten as (see ref [20] for details)

$$\int \sigma_{\gamma^* g} \frac{d\beta}{\beta} \beta G_T(\beta, Q^2). \quad (\text{A6})$$

Thus the integrand in Eq. A2 for the total cross section is positively defined since it is a product of the cross section of the creation of $\bar{q}q$ pair and the structure function of a target. Here $\beta = (Q^2 + M^2)/s$.

It is convenient to rewrite Eq. A6 by expressing the cross section $\sigma(\gamma^* g \rightarrow \bar{q}q)$ through the light-cone wave functions of the virtual photon:

$$\begin{aligned} \sigma &\sim \int \frac{d^2 k_t}{2(2\pi)^3} \int d^2 r_t dz \frac{1}{2(2\pi)^3} \\ &\times \psi(r_t, z) (2\psi(r_t, z) - \psi(r_t + k_t) - \psi(r_t - k_t)) \\ &\times \frac{4 \text{Im} T_{\mu_1\mu_2}^{ab} k^{\mu_1} k^{\mu_2}}{s}. \end{aligned} \quad (\text{A7})$$

Here r_t is the transverse momentum of the constituent within the dipole and k_t is the transverse momentum of the exchanged gluon. The tensor T^{abT} is the sum of the diagrams describing imaginary part of the amplitude for the gluon scattering off the target T. The integral of T^{abT} over $d^2 k_t$ is proportional to the gluon structure function of the target T. The function ψ is the wave functions of the virtual photon. Here r_t is transverse momentum.

Note that the validity of the dipole approximations is becoming better for the larger transverse momenta of the dipole constituents.

Since $r_t \gg k_t$ we can expand the wave functions in the Taylor series:

$$2\psi(r_t, z) - \psi(r_t + k_t) - \psi(r_t - k_t) = -\psi(r_t) \Delta \psi(r_t) k_t^2. \quad (\text{A8})$$

The latter equation is just the equation 2.1:

$$\sigma \sim \int dz \int d^2 r_t \psi(r_t) \Delta \psi(r_t) g((M^2 + Q^2)/s, M^2). \quad (\text{A9})$$

Here $r_t^2/(z(1-z)) = M^2$ and z is the fraction of photon momentum carried by one of the constituents of the dipole.

The resulting cross section can be written either in the momentum representation, giving the representation of the total cross section as the dispersion integral over the invariant masses of the dipoles, or in the coordinate representation, giving the cross section as the integral over the transverse dipole scales.

Similar derivation can be made for the scattering of the spatially small transversely polarized photon. Principal difference is that the contribution of large size $q\bar{q}$ configuration is not suppressed in the case of transversely polarized photon -leading to the aligned jet model.

Let us show now that within the leading logarithmic approximation one can rewrite Eq. A9 in the explicitly positive form. Indeed, let us perform the integration over d^2r_t by parts, using $\Delta = \partial_i \partial_i, i = 1, 2$. The resulting expression contains four terms:

$$\begin{aligned} \sigma \sim & \int dz \left(\int d^2r_t \partial_i \psi \partial_i \psi g((Q^2 + M^2)/s, 4r_t^2) + \int d^2r_t \partial_i \psi \psi(r_t) \partial_i g((M^2 + Q^2)/s, 4r_t^2) \right. \\ & \left. + \text{boundary terms from } r_t \rightarrow 0 + \text{boundary terms, from } r_t \rightarrow \infty. \right) \end{aligned} \quad (\text{A10})$$

Here for the convenience we use definition: $g = xG$. Let us compare the relative contributions of the second and first terms. The ratio of the corresponding integrands is determined by the ratio of derivatives of the logarithms of the wave function and of the structure function. The differentiation ($d/d(r_t^2)$) removes one $\log(r_t^2)$ from the pQCD series over the powers of $\alpha_s \log(r_t^2)$ describing the pQCD evolution of parton distributions. As a result the logarithmic derivative of parton distribution is suppressed by α_s . Hence in the leading logarithmic approximation the second term is parametrically smaller than the first one and can be neglected. Now consider the boundary term. The first of the boundary terms corresponds to the contribution of the small momenta (of $r_t \rightarrow 0$), i.e. to the aligned jet model contribution. This contribution is known to be small for σ_L . (It is zero within the parton model approximation). The second boundary term corresponds to the contribution of the very small dipoles, and clearly is zero since the $\psi \partial_i \psi G \rightarrow 0$ as $r_t \rightarrow \infty$. We conclude, that in the leading logarithmic approximation only the first term should be retained, and we come to Eq. 2.3 in section 2 in the main text.

APPENDIX B: THE ALIGNED JET MODEL (AJM)

The purpose of this appendix is to remind a reader the basic formulae used to calculate the contribution of the AJM model to a total DIS cross sections and forward amplitude of DVCS process in the section 4. The contribution of the aligned jet model to the total cross section initiated by the transversely polarized virtual photon has been evaluated in [30]:

$$\sigma_T = \int_0^{0.7s} dM^2 \frac{M^2}{(M^2 + Q^2)^2} \sigma_{VN}(s/s_0)^{0.08} (\theta(M_0^2 - M^2) + \frac{3u}{M^2} \theta(M^2 - M_0^2)). \quad (\text{B1})$$

Here u is the upper cut off, M_0^2 is a characteristic hadronic scale of the order 1GeV^2 . The first term in the formula corresponds to the contribution of the vector meson dominance

model and it is HT effect, while the second term is the aligned jet model contribution. Since our interest in this Appendix is focussed on moderately large Q^2 we use $R(M^2) \equiv \rho(e^+e^- \rightarrow \text{hadrons})/\rho(e^+e^- \rightarrow \mu^+\mu^-) = 2$. The contribution of charm is not large but requires special treatment. We assume that the cross section for the interaction of hadronic size $q\bar{q}$ pair with a nucleon target depends on collision energy as the soft Pomeron exchange, that the AJM and meson - nucleon cross sections are equal. The cross section of vector meson-proton interaction $-\sigma_{Vp}$ is taken to be ~ 25 mb at the energies of the order $s_0 \sim 400$ GeV².

The contribution of the AJM model to the longitudinal model cross sections is suppressed by a factor $4 * u/Q^2$, i.e.

$$\sigma_{\text{LAJM}} \sim \frac{4u}{Q^2} \sigma_{\text{T AJM}} \quad (\text{B2})$$

APPENDIX C: THE CHARACTERISTIC TRANSVERSE MOMENTA IN THE BLACK DISK LIMIT.

Let us now evaluate the scale of the black disc limit where the partial wave for the forward scattering amplitude reaches 1. This scale gives us the biconcave shape of the nucleon, as it is explained in the section 5.

The black disk scale was discussed already in a number of papers (see e.g. Ref. [16] for the recent discussion and references). Here we remind for a reader the rules of the calculation of the black scale in the dipole model, discuss it's dependence on energy. In order to calculate the corresponding M^2 we need to calculate the partial wave for a dipole -target scattering at zero impact parameter and then impose a black disc limit condition: the partial wave should be 1. (The scale of black disc limit depends on the impact parameter, so in the analysis below we shall consider the case of the zero impact parameter, for larger impact parameters the black disc limit arises at higher energies (see section 6).

Let us define in the standard way the profile function for the dipole scattering:

$$\Gamma(s, b) = \frac{1}{2is(2\pi)^2} \int d^2q_t \exp(i\vec{q}\vec{b}) A(s, t) \quad (\text{C1})$$

Here $t = -q_t^2$, and $A(s, t)$ is the amplitude of the dipole scattering on the nucleon with the momentum transfer q . The elastic, inelastic and total crosssections are connected with this profile function as

$$\begin{aligned} \sigma_{\text{tot}}(s) &= 2 \int d^2b \text{Re}\Gamma(s, b) \\ \sigma_{\text{el}}(s) &= \int d^2b |\Gamma(s, b)|^2 \\ \sigma_{\text{in}}(s) &= \int d^2b (2\text{Re}\Gamma(s, b) - |\Gamma(s, b)|^2). \end{aligned} \quad (\text{C2})$$

The amplitude of dipole nucleon scattering can be expressed through the total cross section and gluon density

$$A(s, t) = is\sigma(s)F_g(t). \quad (\text{C3})$$

Here $\sigma(s)$ is given by Eq. 1.2 with $F^2 = 4/3$ for the fermion dipole and $F^2 = 9/4$ for the gluonic dipole. The two-gluon form factor of the nucleon can be parametrized as to satisfy mainstream ideas on nucleon form factors:

$$F_g(t) = \frac{1}{(1 - t/m_g^2)^2}. \quad (C4)$$

For the numerical dependence of the two-gluon nucleon form factor parameter m_g^2 we shall use the parametrization [15]

$$m_g^2(x, M^2) = m_g^2(x, Q_0^2)(1 + 1.5 \log(Q^2/Q_0^2))^{0.009 \log(1/x)}, \quad (C5)$$

where

$$m_g^2(x, Q_0^2) = 8/C, C = \max(0.28 \text{fm}^2, 0.031 f m^2 + 0.0194 \log(0.1/x) \text{fm}^2), \quad (C6)$$

and $1 f m^2 = 0.04 \text{ GeV}^{-2}$. Qualitatively, $m_g^2 \sim 1 \text{ GeV}^2$.

This parametrization is based on the fit of cross sections of hard diffractive processes in the kinematical domain: $x_B \sim 10^{-4} - 10^{-1}$ and Q^2 up to 10^4 GeV^2 made in ref.[15] and was used in ref. [16] for the analysis of LHC collisions.

Since absorption can not exceed 100% :

$$\Gamma(s, b) \leq 1 \quad (C7)$$

Let us make the Fourier transform of the form factor C4 into impact parameter space :

$$F(b) = (1/2\pi)^2 \left(\int d^2q \exp(i\vec{q}\vec{b}) (m_g^4/(m_g^2 + q_t^2)^2) \right) = (1/2\pi)^2 \frac{m_g^3 b K_1(m_g b)}{4\pi} \quad (C8)$$

Then the condition of probability conservation (of 100% absorption) can be rewritten as

$$\Gamma(s, b) = \frac{\sigma(s) m_g^2}{4\pi} \frac{m_g b}{2} K_1(m_g b) \leq 1 \quad (C9)$$

Note that described above approach to the probability conservation differs from the saturation models which explore formulae of LO BFKL approximation derived for hard processes with one scale and accounted for the conservation of probability in terms of elastic eikonal approximation. (For the recent review see [48, 49]) .Our approach is based on the DGLAP formulae derived for two scale (hard-soft scales) processes like total cross section of DIS and on the condition of complete absorption whose validity does not require applicability of eikonal approximation. Note also that in QCD inelastic diffraction in the scattering of spatially small dipole is significantly larger than elastic one [15]. For many phenomena (but not for all) both approaches lead to qualitatively similar but quantitatively different predictions . Another advantage of the approach used in the paper is in the exploring impact parameter gluon distribution which follows from the two gluon form factor measured in the hard diffractive processes [15].

The typical dependence of the BDR onset scale k_b^2 on energy is presented in Table 5 for the gluonic dipole scattering off a proton target, and in table 6 for fermionic dipole, where we used a CTEQ5 structure functions, the use of CTEQ6 leads to similar results. We consider two possible criterions for reaching the black disk limit: one when the partial

wave Γ at the central impact parameter reaches 1, another when it reaches $1/2$ [15]. Indeed, when the partial wave reaches $1/2$ the probability of inelastic interactions reaches $3/4$, i.e. interactions become strong and pQCD can not be used any more [15].

Let us note that the interaction of quark dipoles (see table 6) is far from the black disk regime for HERA energies, although nonperturbative effects (corresponding to $\Gamma = 1/2$) seem to start to appear for $k_t < 1$ GeV. The results in tables 5,6 are in good agreement with the previous determination of these scales [13, 15, 46].

For our purposes it will be important to determine the rate of increase of the k_b^2 . This rate does not depend on the type of the dipole (fermionic or gluonic) or on the partial wave condition.

For the gluonic dipole in DIS for s up to $s \sim 10^7$ GeV² the BDR scales increase relatively slow as $s^{0.27}$ for CTEQ6 and $s^{0.3}$ for CTEQ5 parametrisation. However at the energies above $s \sim 10^7$ GeV² the increase speeds up with $M^2 \sim s^n$, $n = 0.35$ starting from $s \sim 10^8$ GeV² energies, $n=0.32$ for the exponent for CTEQ6 parametrisation. The CTEQ5 parametrisation leads to even more rapid increase with the energy with $n \sim 0.4$.

APPENDIX D: THE PARAMETRISATION OF THE GLUON DISTRIBUTION FUNCTION

Throughout this paper we use the following approximate formulae for CTEQ5L and CTEQ6L distribution functions.

The CTEQ5L distributions has been shown to be in good agreement with HERA data [16], in the range of $x \sim 10^{-3}, 10^{-4}$. To extrapolate to very small x , we shall use the approximate formulae in the form:

$$g \sim a(M^2)/x^{c(M^2)}. \quad (D1)$$

Here the functions

$$a(M^2) = 2.00123 - 1.69772 \cdot 10/M^2 + 3.07651/\sqrt{M^2/10} - 0.228087 \cdot \log(M^2/10), \quad (D2)$$

$$c(M^2) = 0.045 \log(M^2) + 0.17, \quad (D3)$$

where M^2 is in GeV². This formula is also the good fit to the observed behavior of the structure functions measured at HERA for $150\text{GeV}^2 \geq Q^2 \geq 3 \text{ GeV}^2$, made by ZEUS and H1 collaborations [50].

For CTEQ6 we have similar approximation, but with

$$a(M^2) = 3.96 - 0.032 \cdot 10/M^2 - 1.82/\sqrt{M^2/10} - 0.527 \cdot \log(M^2/10), \quad (D4)$$

$$c(M^2) = 0.035 \log(M^2) + 0.2, \quad (D5)$$

The CTEQ6 distribution is qualitatively similar to CTEQ5 but grows slightly more slow, and is in better agreement with the $J\Psi$ production data.

APPENDIX E: APPROXIMATE FORMULAE FOR THE MEDIAN TRANSVERSE MOMENTA.

For longitudinal photons it is easy to see that the results in a Table 1 with a very good accuracy can be described by an approximate formula

$$4k_t^2 = \frac{a(Q^2)}{(x/0.01)^{0.04+0.02\log(Q^2/Q_0^2)}},$$

$$a(Q^2) = 0.6\text{GeV}^2 + 0.1Q^2.$$
(E1)

Here $Q_0^2 = 10 \text{ GeV}^2$.

For the transverse photons the analysis of Table 2 gives an approximate formula

$$k_t^2 = \frac{a(Q^2)}{(x/0.01)^{0.09+0.014\log(Q^2/Q_0^2)}},$$

$$a(Q^2) = 0.8\text{GeV}^2 + 0.025Q^2.$$
(E2)

The invariant masses increase slightly more slowly, with $M^2(x \sim 0.01) \sim 0.95Q^2 + 9\text{GeV}^2$, and $M^2 \sim 1/(x/0.01)^{0.07+0.015\log(Q^2/Q_0^2)}$, Here $Q_0^2 = 5 \text{ GeV}^2$. If we use the CTEQ5 we obtain qualitatively the same results as in Eq. E2 but the exponent is slightly larger $4k_t^2 \sim 1/x^{0.08+0.001\log(Q^2/Q_0^2)}$, and the invariant masses increase also more rapidly, like $M^2 \sim (0.95Q^2 + 9\text{GeV}^2)/(x/0.01)^{0.08+0.015\log(Q^2/Q_0^2)}$.

-
- [1] S. J. Brodsky, L. Frankfurt, J. F. Gunion, A. H. Mueller and M. Strikman, Phys. Rev. D50 (1994) 3134.
 - [2] H. Abramowicz, L. Frankfurt and M. Strikman, Surveys in High Energy Physics, 11 (1997) 51.
 - [3] L. Frankfurt, G.A. Miller, M. Strikman, Ann. Rev. Nucl. Part. Sci., 44 (1994) 501.
 - [4] B. Blaettel, G. Baym, L. Frankfurt and M. Strikman, Phys. Rev. Lett., 70 (1993) 896.
 - [5] A. H. Mueller Nucl. Phys. B **415**, (1994) 373 .
 - [6] J.C. Collins, L. Frankfurt and M. Strikman, Phys. Rev. D56 (1997) 2982.
 - [7] G. Altarelli and G.Parisi, Nucl. Phys., B126 (1977) 298; V.N. Gribov and L. N. Lipatov, Sov. J. of Nucl. Phys., 15 (1972) 438,672; Yu.L. Dokshitser, Sov. Phys. JETP 46 (1977) 641.
 - [8] S. Catani, M. Ciafaloni, F. Hautmann, Nucl. Phys. B366 (1991) 135.
 - [9] J. Collins, K. Ellis, Nucl. Phys., B360 (1991) 3.
 - [10] V. N. Gribov, Space-time description of hadron interactions at high-energies. In *Moscow 1 ITEP school, v.1 'Elementary particles'*, 65,1973. e-Print: hep-ph/0006158.
 - [11] E. Kuraev, V. Fadin, L. Lipatov, Sov. Phys.-JEP, 44 (1976) 443; 45 (1977) 199. I. Balitsky and L. Lipatov, Sov. J. Nucl. Phys., 28 (1978) 822.
 - [12] L. Frankfurt and V. Sherman, Phys. Lett., 61B (1976) 70.
 - [13] T. C. Rogers, A. M. Stasto and M. I. Strikman, Unitarity Constraints on Semi-hard Jet Production in Impact Parameter Space,”arXiv:0801.0303 [hep-ph].
 - [14] V. Guzey, L. Frankfurt, M. Strikman, M.McDermott, Eur.J. of Physics, C16 (2000) 641.
 - [15] L. Frankfurt, M. Strikman and C. Weiss, Ann.Rev.Nucl.Part.Sci.55 (2005) 403-465.
 - [16] T. C. Rogers and M. I. Strikman, Hadronic interactions of ultra-high energy photons with protons and light nuclei in the dipole picture,” J. Phys. G **32**, (2006) 2041.
 - [17] V.S. Fadin, hep-ph/9807528.
 - [18] F. Caporale, A. Papa, A. Sabio Vera, E. J. of Physics,C53 (2008) 525.
 - [19] L. Frankfurt and M. Strikman, Phys. Rept., 160 (1988) 235.
 - [20] L. Frankfurt, A.Radyushkin, M. Strikman, Phys. Rev. D55(1997) 98.
 - [21] V. N. Gribov, Sov. Phys. JETP 30 (1969) 709.
 - [22] T.H. Bauer, R.D. Spital, D.R. Yennie , F.M. Pipkin, Rev.Mod.Phys.50 (1978) 261, Erratum-ibid.51(1979) 407.
 - [23] Yu. Dokshitzer,D. Diakonov and S. Troyan, Phys. Reports, 58 (1980) 269.
 - [24] M. Abramowitz and I. Stegun, Handbook of special functions,Dover Publications, New York,1964.
 - [25] Deep Inelastic Scattering at the TeV Energy Scale and the LHeC Project. Paul Newman, (Birmingham U.) . Feb 2009. 13pp. To appear in the proceedings of Ringberg Workshop on New Trends in HERA Physics 2008, Ringberg Castle, Tegernsee, Germany, 5-10 Oct 2008. Published in Nucl.Phys.Proc.Suppl.191:307-319,2009. e-Print: arXiv:0902.2292 [hep-ex]
 - [26] G. Altarelli, S. Forte, R.D. Ball, Nucl. Phys., B621 (2002) 359; B674 (2003) 459.
 - [27] M. Ciafaloni, P. Colferai, G.P. Salam, A. M. Stasto, Phys. Lett., 587 (2004) 87; Phys. Rev. D68 (2003) 114003.

- [28] L. Frankfurt, A. Freund, V. Guzey and M. Strikman, Phys. Lett., B418 (1998) 345; Erratum-ibid, B429 (1998) 414.
- [29] L. Frankfurt, A. Freund and M. Strikman, Phys. Rev. D58 (1998) 114001; Erratum D59 (1999) 119901.
- [30] L. Frankfurt and M. Strikman, Nucl. Phys., B316 (1989) 340.
- [31] L. Schoeffel, Phys. Lett., B658 (2007) 33.
- [32] A. Aktas et al, Eur. Phys. J., C48 (2006) 715; S. Chekhanov et al, arXiv:0812.2003 (hep-ex).
- [33] V. Guzey, L. Frankfurt, M. Strikman, M. McDermott, Phys. Rev. Lett., 87 (2001) 192301.
- [34] L. Frankfurt, M. Strikman and C. Weiss, Phys. Rev. D **69**, (2004) 114010.
- [35] L. B. Ioffe, V. Gribov, I. Pomeranchuk, Sov. J. of Nucl. Phys., 2 (1966) 549.
- [36] B. L. Ioffe, Phys. Lett., B30 (1969) 123.
- [37] Y. Kovchegov and M. Strikman, Phys. Lett., B516(2001) 314.
- [38] B. Blok and L. Frankfurt Phys. Lett. B630 (2005) 49-57.
- [39] B. Blok, L. Frankfurt, M. Strikman, arXiv:0811.3737 (hep-ph)
- [40] A. H. Mueller, Nucl. Phys. A702 (2003) 65-72.
- [41] A. Dumitru and J. Jalilian-Marian, Phys. Rev. Lett. **89**, (2002) 022301 [arXiv:hep-ph/0204028].
- [42] D. Diakonov and V. Y. Petrov, Nucl. Phys. B **272** (1986) 457 .
- [43] L. Frankfurt, V. Guzey and M. Strikman, Phys. Rev. D **71**, (2005) 054001.
- [44] A. Bohr and B. R. Mottelson, Nuclear structure, v.1, W. A. Benjamin, New York, 1969.
- [45] L. Frankfurt , M. Strikman , M. Zhalov Phys. Lett. B616 (2005), 59-75.
- [46] L. Frankfurt and M. Strikman, in Phys. Reports, 455 (2008) 105.
- [47] V. N. Gribov The theory of complex angular momenta: Gribov lectures on theoretical physics. Cambridge, UK: Univ. Pr. (2003).
- [48] L. McLerran and R. Venugopalan, Physical Review, D49 (1994), 2233, 3352; D50 (1994) 2225; D59 (1999) 094002; see also L. McLerran, Surveys High Energy Phys., 18 (2003) 101; Nucl. Phys. A702 (2002) 49, for the latest reviews on the subject.
- [49] A. H. Mueller Nucl. Phys. B **415**, (1994) 373.
- [50] C. Adloff et al, Phys. Lett., B520 (2001) 183; S. Chekanov et al, Nucl. Phys. B713 (2005) 3.

	$Q^2 = 3 \text{ GeV}^2$	5 GeV ²	10 GeV ²	20 GeV ²	40 GeV ²	60 GeV ²	80 GeV ²	100 GeV ²
$s = 10^{-3} \text{ GeV}^2$	0.82 GeV ²	1.1 GeV ²	1.8 GeV ²	3.14 GeV ²	5.5 GeV ²	7.75 GeV ²	9.9 GeV ²	11.9 GeV ²
$s = 10^{-4} \text{ GeV}^2$	0.90 GeV ²	1.25 GeV ²	2.1 GeV ²	3.65 GeV ²	6.5 GeV ²	9.3 GeV ²	11.9 GeV ²	14.5 GeV ²
$s = 10^{-5} \text{ GeV}^2$	0.95 GeV ²	1.35 GeV ²	2.3 GeV ²	4 GeV ²	7.2 GeV ²	10.2 GeV ²	13.15 GeV ²	16 GeV ²
$s = 10^{-6} \text{ GeV}^2$	1.01 GeV ²	1.46 GeV ²	2.5 GeV ²	4.4 GeV ²	7.9 GeV ²	11.2 GeV ²	14.5 GeV ²	17.6 GeV ²
$s = 10^{-7} \text{ GeV}^2$	1.08 GeV ²	1.61 GeV ²	2.7 GeV ²	4.8 GeV ²	8.65 GeV ²	12.3 GeV ²	15.9 GeV ²	19.4 GeV ²

TABLE I: The scale k_{t1}^2 (50% of the total cross section) for longitudinal photons in DIS (CTEQ6)

	$Q^2 = 3 \text{ GeV}^2$	5 GeV ²	10 GeV ²	20 GeV ²	40 GeV ²	60 GeV ²	80 GeV ²	100 GeV ²
$s = 10^{-3} \text{ GeV}^2$	0.91 GeV ²	1.07 GeV ²	1.35 GeV ²	1.78 GeV ²	2.3 GeV ²	2.75 GeV ²	3.06 GeV ²	3.45 GeV ²
$s = 10^{-4} \text{ GeV}^2$	1.18 GeV ²	1.42 GeV ²	1.82 GeV ²	2.42 GeV ²	3.25 GeV ²	3.9 GeV ²	4.4 GeV ²	5 GeV ²
$s = 10^{-5} \text{ GeV}^2$	1.37 GeV ²	1.67 GeV ²	2.18 GeV ²	2.98 GeV ²	4.1 GeV ²	5. GeV ²	5.8 GeV ²	6.5 GeV ²
$s = 10^{-6} \text{ GeV}^2$	1.54 GeV ²	1.91 GeV ²	2.57 GeV ²	3.57 GeV ²	5. GeV ²	6.3 GeV ²	7.3 GeV ²	8.3 GeV ²
$s = 10^{-7} \text{ GeV}^2$	1.76 GeV ²	2.21 GeV ²	2.95 GeV ²	4.3 GeV ²	6.2 GeV ²	7.9 GeV ²	9.35 GeV ²	10.5 GeV ²

TABLE II: The scale k_{t1}^2 (50% of the total cross section) for transverse photons in DIS (CTEQ6)

	$Q^2 = 3 \text{ GeV}^2$	5 GeV ²	10 GeV ²	20 GeV ²	40 GeV ²	60 GeV ²	80 GeV ²	100 GeV ²
$x = 10^{-2} \text{ GeV}^2$	38	45	50	56	60	61	62.5	63
$x = 10^{-3} \text{ GeV}^2$	61	66	71	75	78	80	80.5	81
$x = 10^{-4} \text{ GeV}^2$	73	81	84	84.5	87	88	88.5	89
$x = 10^{-5} \text{ GeV}^2$	81	84	87.5	90	92	92.5	93	93.5
$x = 10^{-6} \text{ GeV}^2$	87	89.5	92	94	95	95.5	96	96
$x = 10^{-7} \text{ GeV}^2$	91	93	95	96	97	97.3	97.6	98

TABLE III: The pQCD contribution (%) in the total cross section, that includes AJM contribution (CTEQ6)

	$Q^2 = 5 \text{ GeV}^2$	10 GeV^2	20 GeV^2	40 GeV^2	60 GeV^2	80 GeV^2	100 GeV^2
$x = 10^{-2} \text{ GeV}^2$	1.93	2.	2.08	2.2	2.26	2.3	2.34
$x = 10^{-3} \text{ GeV}^2$	1.86	1.94	2.02	2.1	2.13	2.15	2.17
$x = 10^{-4} \text{ GeV}^2$	1.74	1.82	1.88	1.92	1.94	1.95	1.97
$x = 10^{-5} \text{ GeV}^2$	1.66	1.72	1.76	1.79	1.8	1.81	1.82
$x = 10^{-6} \text{ GeV}^2$	1.6	1.63	1.67	1.69	1.71	1.72	1.72
$x = 10^{-7} \text{ GeV}^2$	1.52	1.56	1.6	1.62	1.64	1.66	1.66

TABLE IV: The DVCS ratio R (CTEQ6)

	$\Gamma = 1$	$\Gamma = 1/2$
$s = 10^4 \text{ GeV}^2$	1.6 GeV^2	3.1 GeV^2
$s = 10^5 \text{ GeV}^2$	3 GeV^2	5.6 GeV^2
$s = 10^6 \text{ GeV}^2$	6 GeV^2	10 GeV^2
$s = 10^7 \text{ GeV}^2$	11 GeV^2	21 GeV^2

TABLE V: The scale k_t^2 for the onset of the black disk regime for the gluon dipole.

	$\Gamma = 1$	$\Gamma = 1/2$
$s = 10^4 \text{ GeV}^2$	1 GeV^2	1 GeV^2
$s = 10^5 \text{ GeV}^2$	2 GeV^2	2 GeV^2
$s = 10^6 \text{ GeV}^2$	5 GeV^2	5 GeV^2
$s = 10^7 \text{ GeV}^2$	10 GeV^2	10 GeV^2

TABLE VI: The scale k_t^2 for the onset of the black disk regime for the fermionic dipole.

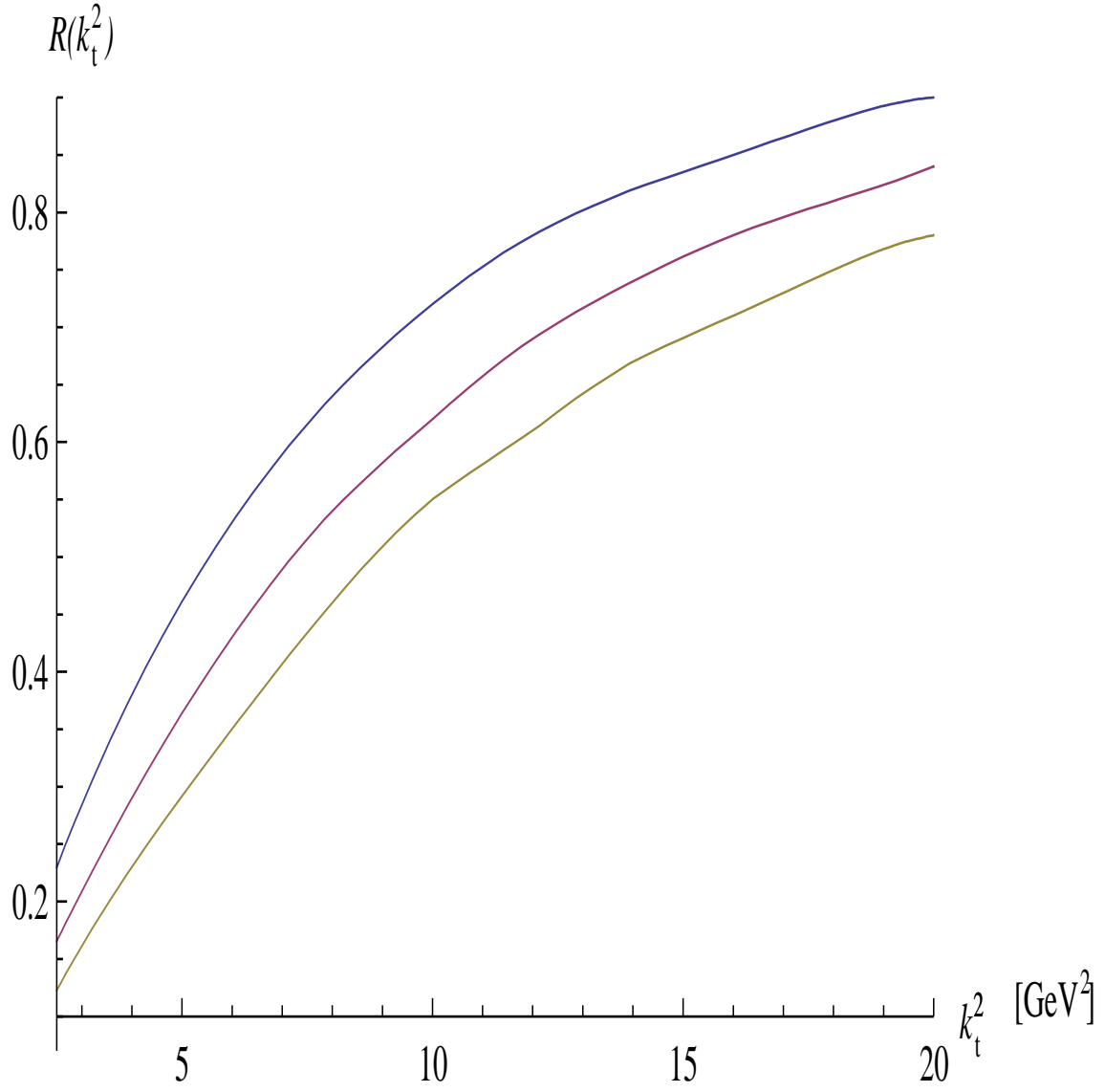


FIG. 1: The ratio $R(k_t^2)$ for $Q^2 = 40 \text{ GeV}^2$ for longitudinal photons. The three curves correspond to $x=10^{-3}$ (upper one), 10^{-5} (middle one) and 10^{-7} (lower one).

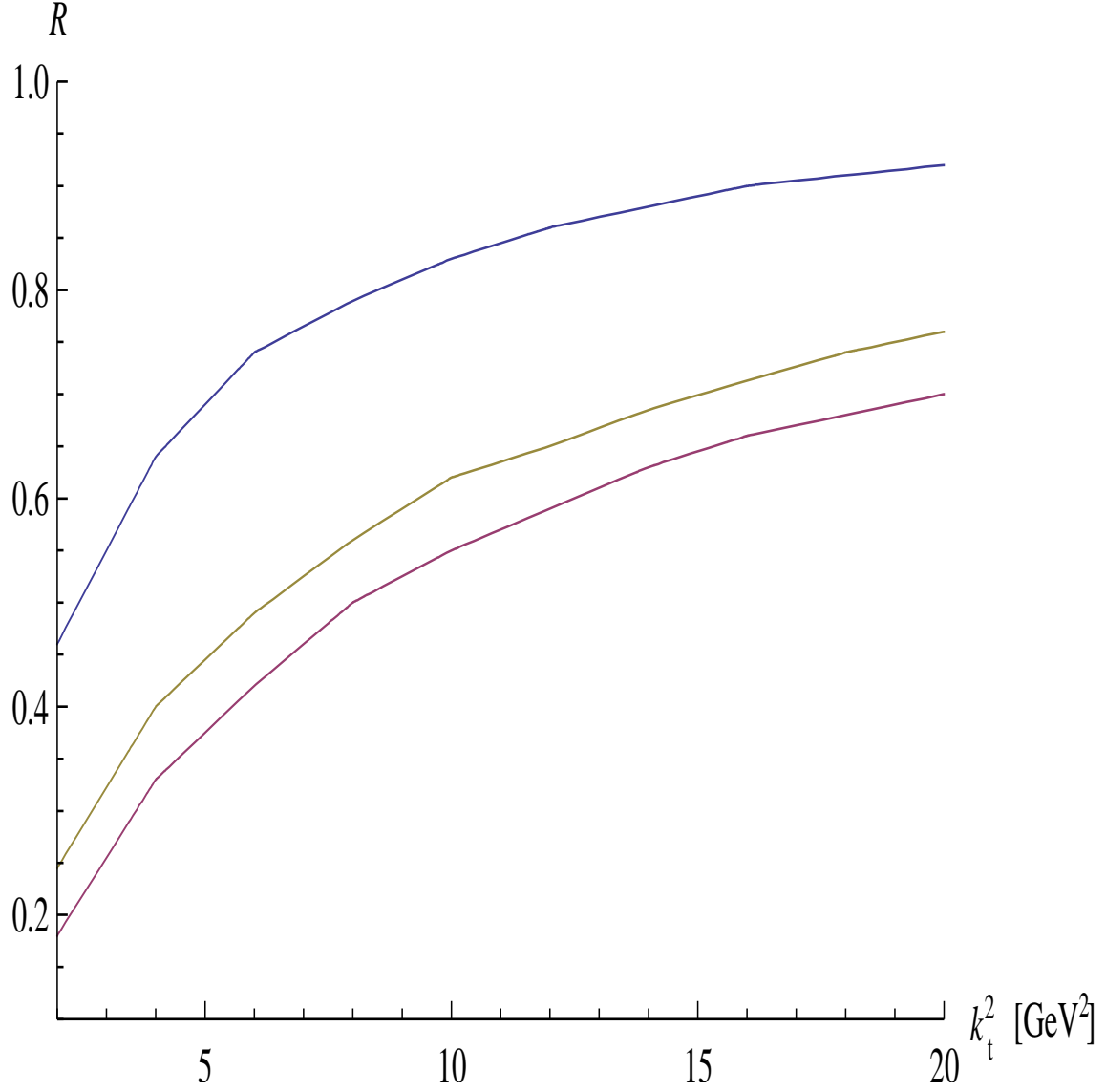


FIG. 2: The ratio $R(k_t^2)$ for $Q^2 = 40 \text{ GeV}^2$ for transverse photons. The three curves correspond to $x=10^{-3}$ (upper one), 10^{-5} (middle one) and 10^{-7} (lower one).

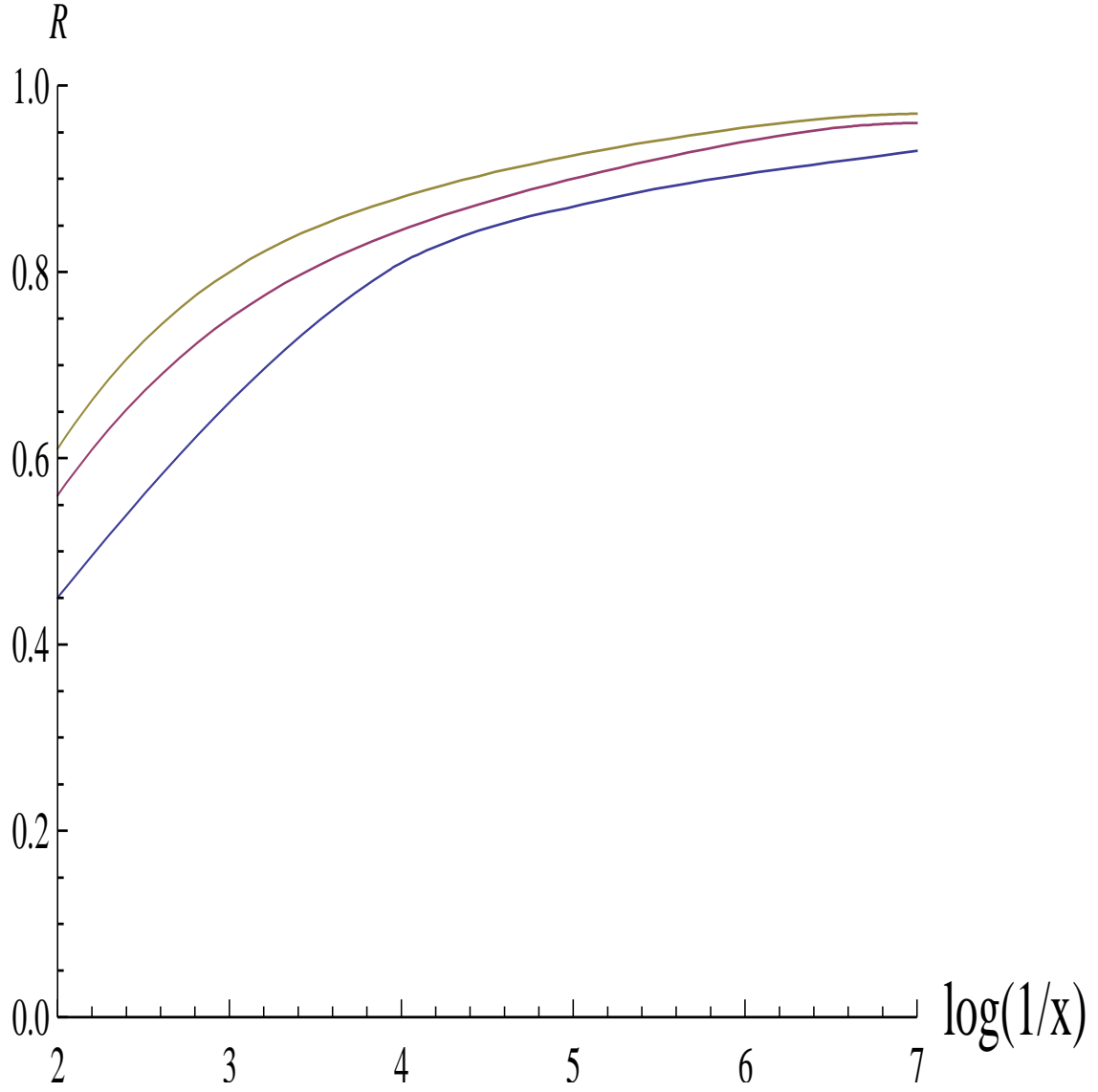


FIG. 3: The contribution R of pQCD to the total cross section, that is a sum of pQCD and AJM model contributions. The cut off of the AJM model is 0.35 GeV^2 , for $Q^2 = 5 \text{ GeV}^2$ (lower curve), 20 GeV^2 (middle curve), 40 GeV^2 , the x axis corresponds to $\log_{10}(1/x)$

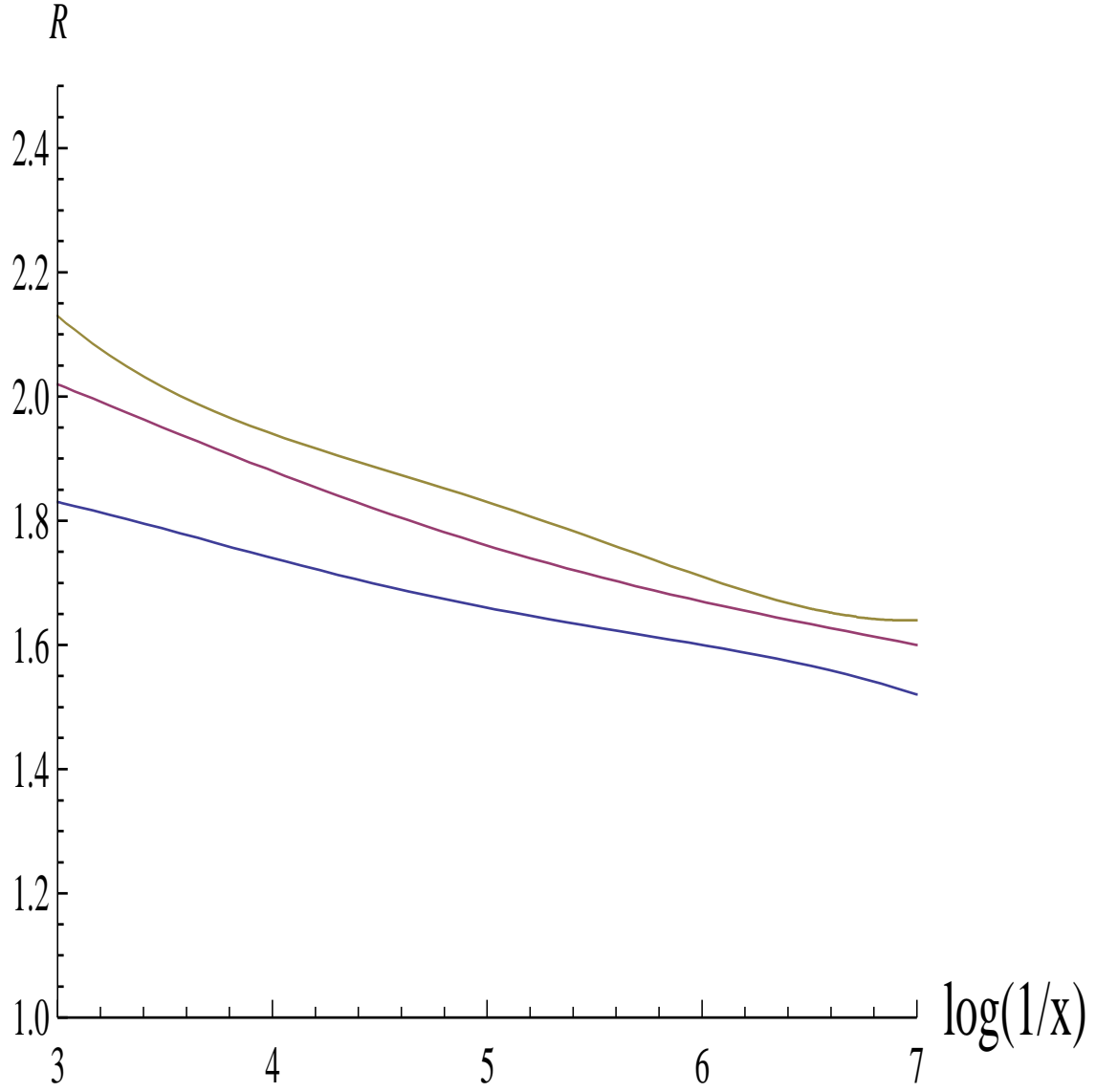


FIG. 4: The ratio R of the DVCS cross section to total transverse cross section for different values of Q^2 as a function of x_B . for $Q^2 = 5 \text{ GeV}^2$ (lower curve), 20 GeV^2 (middle curve), 60 GeV^2 (upper curve), the x axis corresponds to $\log_{10}(1/x)$

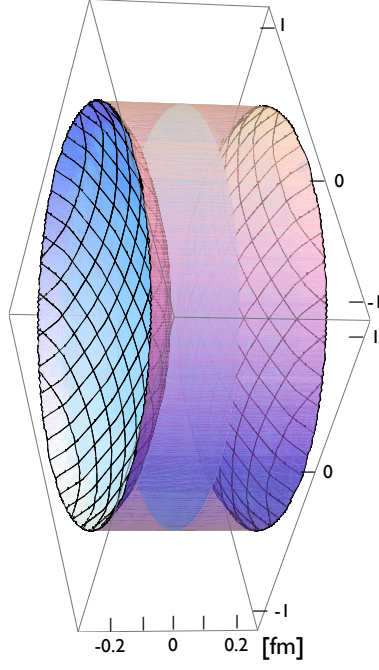


FIG. 5: 3D image of the fast nucleon at $s = 10^7 \text{ GeV}^2$ and the resolution scale $Q^2 \leq 40 \text{ GeV}^2$,

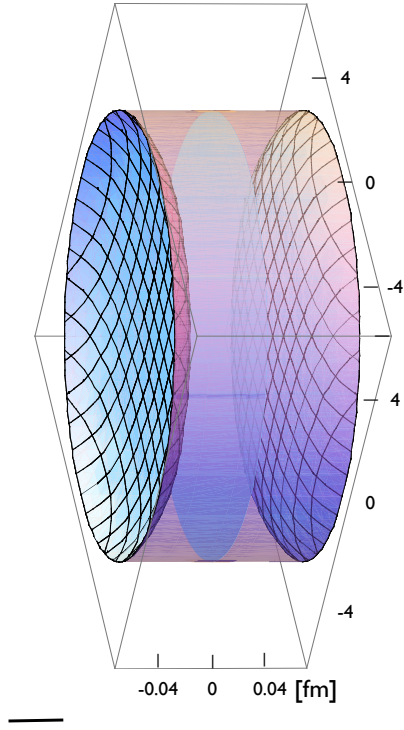


FIG. 6: 3D image of the fast heavy nucleus (gold) at $s = 10^7 \text{ GeV}^2$ and the resolution scale $Q^2 \leq 40 \text{ GeV}^2$. Let us stress that the thickness of a nuclei in the Figure is much smaller than the thickness of the nucleon.